Norwegian University
of Life Sciences

Master's Thesis 2023 60 ECTS
Faculty of Biosciences

The genomic basis of lipid accumulation in *Mucor circinelloides* VI 04473

Veronica Aarvik Bøe
M.Sc. Genome Science

Acknowledgements

In this master thesis, the competence of the Faculty of Science and Technology in gas chromatography and spectroscopy has been combined with the genomic science and bioinformatical skillsets at the Faculty of Biosciences at NMBU. These combined strengths have assisted in investigating the genomic basis of lipid accumulation in *Mucor circinelloides* VI 04473 under calcium deprived conditions.

First, I would like to thank my supervisor and co-supervisors: Volha Shapaval, Simen Rød Sandve and Helle Tessand Baalsrud. Thank you for all your guidance, input, assistance in analyses, and encouraging words throughout this project. By setting aside time for meetings and discussions from an early point on, you have helped me navigate through this (sometimes overwhelming) process that a master thesis can be.

I would also like to thank Dana Byrtosova for being a great mentor in the lab! Not only have you assisted us in the practical lab work and analyses, but you have also provided thorough and educational answers to all my questions regarding fungal biology. Finally, a thank you to Thu-Hien for the work you have put into the genome assembly and annotation for this project.

Veronica Aarvik Bøe

Sammendrag

Den dimorfe muggsopparten *Mucor circinelloides* kan akkumulere opp til 80% av ens egen biomasse i lipider som er av interesse for ernæring og fór (som for eksempel flerumettede fettsyrer). Derfor er den et lovende alternativ til dyr og planter som råmateriale. Å optimere utbyttet er dermed av stor industriell interesse. Dzurendova et al. (2021b) viste at fravær av kalsium, kombinert med ulike nivå av fosfor, økte lipid-produksjonen i *Mucor circinelloides* VI 04473. Målet med denne avhandlingen var å undersøke det genomiske grunnlaget for lipid akkumulering, og den regulatoriske gen-responsen på fravær av kalsium, i MC VI 04473. Fenotypiske data fra gasskromotografi og Fouriertransformasjon infrarød spektroskopi kombinert med genuttrykksdata fra RNA sekvensering ble analysert.

Fenotypiske data viste at den største økningen i lipidakkumulering forekom i behandlingen hvor kalsium-fravær ble kombinert med lave nivå av fosfor. Interessante funn av nedregulerte gener i denne behandlingen omfattet nedbrytning av fettsyrer, lipid signalisering, lipid transport, og kalsium-bindende proteiner. Interessante funn blant oppregulerte gener var relatert til cellevekst, polyfosfat- og karbohydrat-metabolisme, og stresstoleranse.

Analysen av differensielt uttrykte gener mellom kalsium-fravær og kalsium-nærvær resulterte i utpekningen av enkelte gener som var relatert til både lipidakkumulering og kalsium-fravær. Dog, videre forskning kreves for å kunne belyse sammenhengen mellom kalsium og lipidakkumulering. Forbedring av genom-annotasjonen til MC VI 04473 kan bidra til å belyse denne sammenhengen.

Summary

The filamentous dimorphic fungi *Mucor circinelloides* can accumulate up to 80% of its biomass in lipids of interest to feed and nutrition (like polyunsaturated fatty acids). This makes it a promising raw material alternative to animals and plants. Optimizing the lipid yield is therefore of great industrial interest. Dzurendova et al. (2021b) demonstrated that calcium starvation, combined with different levels of phosphorus, increased the lipid production in *Mucor circinelloides* VI 04473. The aim of this thesis was to investigate the genomic basis of lipid accumulation, and the gene regulatory response to calcium starvation in MC VI 04473. Phenotypic data from gas chromatography and Fourier-transform infrared spectroscopy combined with gene expression data from RNA sequencing was analyzed.

Phenotypic data showed that the greatest increase in lipid accumulation occurred in the treatment with a combination of calcium starvation and low level of phosphorus. Interesting findings in downregulated genes under this treatment included degradation of fatty acids, lipid signaling, lipid transportation and calcium binding proteins. In upregulated genes, findings were related to cellular growth, polyphosphate and carbohydrate metabolism and stress resistance.

The analysis of differentially expressed genes between absence of calcium and presence of calcium resulted in the identification of some genes relevant to both lipid accumulation and calcium starvation. However, further studies are needed to elucidate the relationship between calcium and lipid accumulation. Improved genome annotation for MC VI 04473 can assist in further analysis of this relationship.

Table of Contents

Introduction

Fungi play a central role in many areas of life: From their role in the ecosystem as decomposers and plant nutrient providers (mycorrhizae and endophytes), to pathogenic species that pose a threat to individuals and agriculture. Throughout history, some species have also proved to be beneficial for human life – some famous examples are fermenting yeasts and the origin of antibiotics (penicillin). Despite their many impacts on nature and our life, the biology and genetics of fungi is still understudied compared to that of animals and plants (Naranjo-Ortiz & Gabaldón, 2019). It is estimated that there are 2-11 million fungal species, though "only" 150 000 of these has been identified (Phukhamsakda et al., 2022).

One area which especially requires understanding of fungal genes and molecular mechanisms, is the industrial interest in fungal metabolites. Fungi are being investigated as a potential source for production of lipids, organic acids, enzymes, pigments, polyphosphates, ethanol, and chitosan (Dzurendova et al., 2021a). Some species of fungi are oleaginous and can accumulate up to 20 - 80% of its total biomass in lipids (Chen et al., 2015; Dong et al., 2016; Tang et al., 2015). These species have the potential to replace animals and plants as raw materials in the production of polyunsaturated fatty acids (PUFAs), like omega-3 and omega-6, in areas such as feed, medicine, cosmetics and other industries (Patel A et al., 2020). Animals must obtain these through diet, as they cannot synthesize them (Fazili et al., 2022). Fungal lipid production is cost-effective, low-impact, independent of climate and can use a wide variety of carbon sources (Simona Dzurendova et al., 2021a; Ochsenreither et al., 2016).

One of the most known model species for fungal lipid production is *Mucor circinelloides* (MC) (Fazili et al., 2022). In addition to its ability to accumulate lipids, MC has also been investigated as a source of other valuable substances such as polyphosphates and carotenoids (S. Dzurendova et al., 2021b). Fazili et al. (2022) suggested that by lipid transformation, it can also be a raw material source for biodiesel.

Efforts have been made to understand the mechanism behind the lipid accumulation trait, such as genetic modifications and culture manipulations (Mohamed et al., 2021; Nagy et al., 2017; S. Wang et al., 2017). Dzurendova et al. (2021b) demonstrated that calcium availability may play a central role in the ability of MC, as well as other Mucoromycota species, to accumulate lipids. In

this study, MC had increased lipid accumulation as the effect of calcium starvation. Among the Mucoromycota species studied, this was more pronounced in the strain *M. circinelloides* VI 04473 (MC VI 04473). However, the genetic underpinning of the effect of calcium on lipid accumulation is unknown. Based on this observation, this thesis will investigate the lipid accumulation trait in this strain closer, from a genomic perspective.

In this project we conducted an experiment with MC VI 04473 growing at two calcium conditions – one where calcium was absent, and one where calcium was present in a usual concentration. We generated gene expression data using RNA sequencing (RNAseq), which were analyzed together with a complete chromosome-level genome assembly for MC VI 04473.

To determine the relative composition of fungal biomass, lipid content and fatty acid profiles, we used Fourier-transform infrared spectroscopy, the high throughput screening extension (FTIR-HTS) and gas chromatography (GC), respectively. This phenotypic data were combined with differential gene expression analyses to shed light on the following questions:

1. What is the genomic basis of lipid accumulation in MC VI 04473?
2. What is the gene regulatory response to calcium starvation?

Background

The Oleaginous fungi - *Mucor circinelloides*

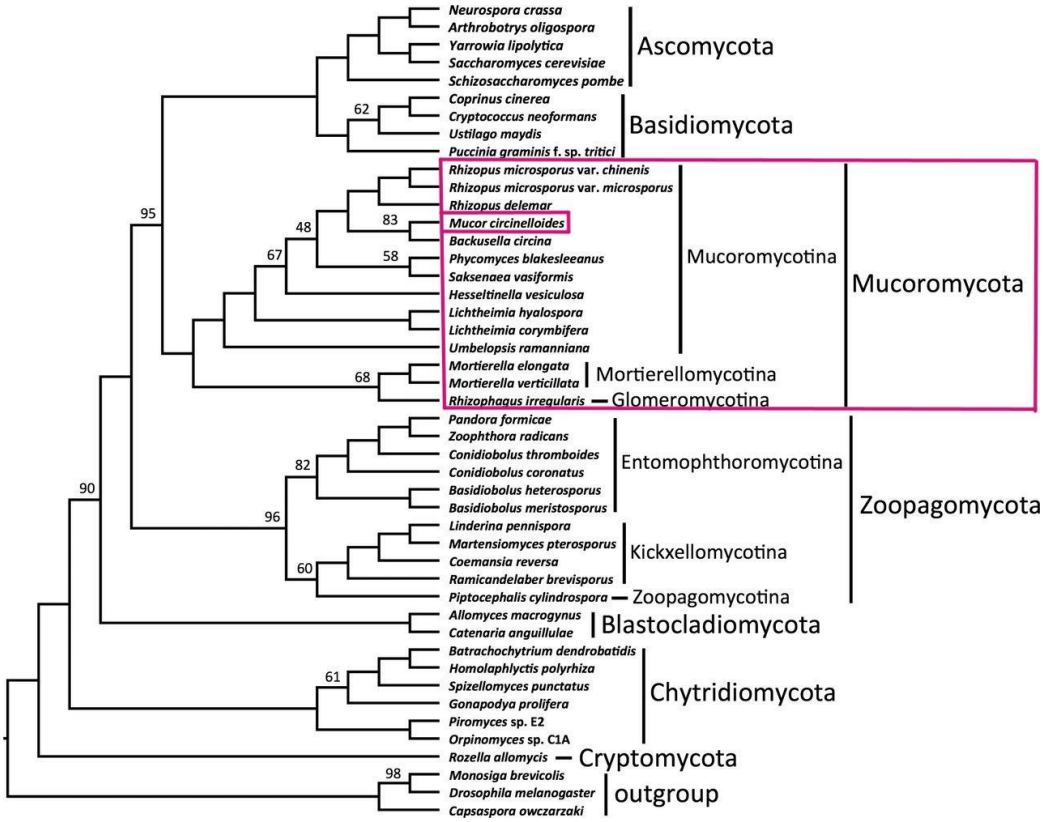

Figure 1 Phylogeny tree of the kingdom Fungi, showing the main phyla and some species within these. The phylum of interest in this thesis, Mucoromycota, is marked by a purple square, as is M. circinelloides. Illustration: Spatafora et al. (2016)

MC belongs to the phylum Mucoromycota, along with other oleaginous species such as *Mortierella*, *Rhizopus* and *Umbelopsis* (Figure 1). Mucoromycyota and Zoopagiomycota were previously grouped together under a single phylum, Zygomycetes, but thanks to rapid advances in the field of genome science over the last 10 years, these phyla are now separate groups (Li et al., 2021). MC is a dimorphic fungus, meaning that it can alternate between filamentous hyphal forms, and spherical budding yeast-like forms (Lübbehüsen et al., 2003). In fungal species with dimorphism, the filamentous stage is multicellular, and the yeast stage is unicellular. MC differs in this, in that both forms can consist of multi-nucleated cells (Wolff et al., 2002). The transition

between the two growth modes can be triggered by environmental conditions, like anerobic conditions (Homa et al., 2022; Lübbehüsen et al., 2003). This dimorphic trait has also been linked to the virulence of MC. Although MC is mainly found in soil as decomposers, mycorrhizal fungi, and root endophytes, it can also be pathogenic to plants, and humans with an impaired immune system (Bonfante & Venice, 2020; Lee et al., 2015).

MC's morphology is closely linked to the ability to accumulate large amounts of lipids. In the hyphae as well as in the yeast-like cells, there are specialized organelles called lipid droplets (Figure 2). The formation of these droplets is a conserved mechanism in eukaryotes (Graef, 2018)**.** Neutral lipids, like triacylglycerols (TAGs) and sterol esters, are found in their core, which is surrounded by a phospholipid monolayer (Graef, 2018; Zan et al., 2018). Usually, they emerge from the endoplasmic reticulum (ER) (Graef, 2018). Their main functions are energy storage and providing precursors for lipid synthesis, but recent years have also revealed that they play a role in cellular metabolism and stress responses, due to their many dynamic interactions within the cell (Danielli et al., 2023). It has been shown thatin dimorphic MC yeast-like cells are prone to the higher accumulation of lipids than hyphae cells (Shapaval et al., 2023).

Figure 2 Hyphae of MC VI 04473, containing lipid droplets (example marked by purple circle). The photo was taken during harvesting of biomass, using a Leica DM6 B microscope (Leica Microsystems, Germany). The sample in this picture was grown under the treatment Ca0P05.

Oleaginous fungi are able to accumulate high levels of lipids in their cells through de novo fatty acid synthesis and lipid assembly pathways

De novo fatty acid (FA) synthesis is a process occurring in the cytoplasm of cells, where fatty acids are synthesized from simple precursors such as acetyl-CoA and malonyl-CoA (Zhang et al., 2022). The principles of fungal lipid synthesis are similar to that of other eukaryotes, as it is a conserved mechanism required for function and structure in the cells (Ochsenreither et al., 2016). It occurs in the cytoplasm, where citrate is converted to acetyl-CoA by ATP citrate lyase. Acetyl-CoA undergoes carboxylation, and malonyl-CoA is formed. Then, a fatty acid synthase, powered by NADPH, converts malonyl-CoA into long-chain fatty acids (palmitic acid or stearic acid). These final products can be stored as TAGs, after transportation to the ER, where they are elongated and desaturated. They can also be converted to cholesterol, or used for synthesis of other lipids, like phospholipids and sphingolipids (Zhang et al., 2022). Fungal lipid production differs from other eukaryotes in some of the enzymes and pathways involved in lipid synthesis. For example, fungal fatty acid synthase and desaturase enzymes are structurally different in fungi (DeJarnette et al., 2021).

There is great interest in optimizing the lipid yield from oleaginous fungi. The accumulation of lipids is influenced by various factors such as carbon and nitrogen sources, temperature, pH, and more recently calcium (Dzurendova et al., 2021b).

Cultivation and nutrition requirements

In nature, microbial fungi are usually not visible to the naked eye, unless it has reached its sporulation stage, where fuzzy spores appear on e.g. old bread and fruit. The rest of the organism is found within soil and organic material. In a natural environment, there are a number of interactions and dynamics affecting the way in which a fungus grows and behaves, like the metabolic activity of other organisms in the environment, nutrition exchange, temperature fluctuations, pH, water, and oxygen availability.

A natural environment is hard to replicate in a laboratory setting. However, adjustments can be made to the growth medium so that the main components, and their ratios (and thus, the pH), fit the nutrition requirements of the species in question. The main component of a growth media for

fungal cultivation consists of: carbon and energy sources (often glucose), nitrogen (from nitrate, ammonium, or amino acids), phosphorus, essential metals (calcium and magnesium), and trace elements (copper, iron, manganese, potassium, nickel, and zinc) (Walker & White, 2011).

A common way of studying fungi metabolism is manipulating the nutrient composition and environmental conditions (incubation temperature, pH, and dissolved oxygen) in the growth media (Zhang et al., 2022). In MC and other oleaginous fungi, nitrogen limitation combined with excess carbon triggers a stress lipogenesis, resulting in an increased amount of accumulated lipids (Ochsenreither et al., 2016; Xia et al., 2011). Phosphorus plays a major role in fungal carbon and amino acid metabolism, adaptation to stress conditions, and polysaccharide biosynthesis (Bhalla et al., 2022). Furthermore, fungi tend to store phosphorus as polyphosphate (polyp) in its cell walls and intracellular granules localized to ER, which has been hypothesized to be linked to pathogenicity due to influence on the cell surface (Bhalla et al., 2022; Dzurendova et al., 2021b). Due to its many roles in fungal cellular processes, experimental designs sometimes involve using different levels of phosphorus in the growth media.

Adjusted levels of metals in growth media is a less common treatment, but not unheard of (Bellou et al., 2016; Fonseca-Peralta et al., 2022). Like previously mentioned, Dzurendova et al. (2021b) found that the availability of calcium ions affected the lipid accumulation. Calcium is an important signaling molecule that influences growth, reproduction, development, virulence, and stress in fungi (Roy et al., 2021). In Dzurendova et al.'s (2021b) experiment, the absence of calcium in combination with different levels of phosphate indicated that the two treatments might interact with one another. Kikuchi et al. (2014) suggested an interaction between phosphate and cations, where the uptake of Na(+) , K(+) , Ca(2+) and Mg(2+) was affected by polyphosphate accumulation. They hypothesized that the negative charge of polyphosphate is neutralized by the cations. They also observed a change of gene expression related to maintenance of cellular homeostasis, mineral uptake, and phosphate and nitrogen metabolism.

As lipid synthesis is a process involving many other pathways and metabolic precursors, it seems not unlikely that calcium- and phosphorus-modifications to the growth media might directly or indirectly affect the lipid accumulation trait. However, to confirm this, further studies are needed.

Genomic basis for lipid accumulation in oleaginous fungi

Lipid synthesis is a complex trait, meaning that it cannot be explained by one gene, but rather several genes, their interactions, and regulatory elements. Despite the great interest in this trait, it is not yet completely understood. Efforts have been made to understand the genomic basis of it (Chen et al., 2015; Tang et al., 2015)

Investigations in the genomic basis of lipid accumulation requires quality genome assemblies and genome annotation. Thanks to the next generation sequencing technologies and evolving bioinformatic tools, assemblies are being rapidly produced and made publicly available. As of this date, 16 draft genomes for MC have been published (NCBI, 2023). It should however be noted that none of these are chromosome level, and MC VI 0447 is not among them.

The existence of assemblies makes comparative genomics and transcriptomic analyses possible. Genes with a potential role in fungal lipid production can be identified by comparing the genome of a high lipid-producing strain, with the genome of a less productive strain. Another approach is to sequence RNA from fungal tissue grown under different experimental conditions. The transcriptome, containing the full range of messenger RNAs, reveals which genes are being expressed in the tissue.

Through genomic approaches, several enzymes and genes have previously been linked to lipid production in fungi. As FA synthesis requires power, providers of NADPH and enzymes involved in carbon flux have been investigated. Malic enzyme (ME) is considered the main provider of NADPH, in addition to glucose-6-phosphate dehydrogenase (G6PD) and dehydrogenase (PGD) (Chen et al., 2015). Genes encoding these enzymes have therefore been considered.

Acetyl-CoA is the precursor of FA synthesis. Therefore, enzymes which assist in providing this (e.g., ATP-citrate lyase, which assists acetyl-CoA in entering the cytosol) have been considered targets for genetic engineering (overexpression) (Chang et al., 2019). The activity of adenosine monophosphate deaminase (AMPD), which is increased by nitrogen limitation, has a cascading effect which eventually results in an accumulation of isocitrate in the mitochondria. This is converted to citric acid, which in turn ends up as acetyl-CoA for FA synthesis (Chang et al., 2019).

AMP-activated protein kinase (AMPK) inactivates acetyl-CoA carboxylase (ACC), which converts acetyl-CoA to malonyl-CoA. Nosheen et al. (2021) identified Snf-β as a gene encoding

the β subunit of AMPK complex in *M. circinelloides* WJ11. Their study showed that manipulation of Snf-β affected the expression of the gene encoding ACC, thereby affecting lipid metabolism.

Yang et al., (2021) noted that fatty acid synthases (fas1 and fas2 genes) and the ATP-citrate lyase gene acl were activated when citrate transporter genes were overexpressed. Additionally, they confirmed the role of *sodit-a* and *sodit-b* as plasma membrane malate transporters, based on previous studies on the role of intracellular malate concentration in lipid accumulation in MC.

The organelles peroxisomes perform β-oxidation of FAs, among other metabolic functions. The role of peroxisomal transporters have therefore been investigated in yeast (Dulermo et al., 2015). Intracellular lipases have also been investigated for their role in degradation of TAGs (Dulermo et al., 2013).

The study of lipid accumulation in MC VI 04473 might reflect some of the general findings above. However, genetic patterns related to lipid accumulation can vary depending on the fungal species. As Tang X et al. (2015) illustrated for the two strains of MC (WJ11 and CBS277.49v2.0), factors leading to up- or downregulation of lipid-related genes might have a different impact even between strains of the same species. This is also pointed out by Dulermo et al. (2015), as unidentified proteins in the species of interest might be at play.

Material and methods

Biomass production of *Mucor circinelloides*

Experimental design

MC VI 04473, provided by the Norwegian School of Veterinary Science (NMBU, Ås, Norway), was cultivated under two different calcium (Ca) conditions and three different concentrations of inorganic phosphorus substrate (P). For the condition Ca1, calcium was present in the medium in a concentration 0.1 g/L and for the condition Ca0, calcium was absent. The selected reference values for the phosphate salts were 7 g/L KH_2PO_4 and 2 g/L Na_2HPO_4, hereby referred to as P1. To have a higher and a lower amount of phosphate salts, the experiment included two additional P-conditions: P4 (4x P1), and P0.5 (0.5x P1).

The combination of the Ca- and P-conditions resulted in the six different treatments – Ca1P1, Ca1P4, Ca1P0.5, Ca0P1, Ca0P4, Ca0P0.5. For each treatment, four biological replicates were produced. A nitrogen-limited broth media was used in combination with Ca-P conditions for each of the six treatments.

Cultivation

Cultivation was carried out according to Dzurendova et al. (2021b), with some minor modifications, such as timespan for growth and concentration of malt extract agar concentration used for preparation of spore inoculum. Each cultivation was performed on a separate day and was considered as a biological replicate.

Preparing spore inoculum

50 g/L of malt extract agar (MEA) was prepared by dissolving 20 g of MEA powder (Merck, Germany) in 400 mL distilled deionized water. The solution was autoclaved at 121 °C for 15 minutes. Sterile MEA agar was used to prepare Petri dishes which were used to inoculate *Mucor circinelloides* by transferring three 5 µL of stock spore solution (kept at -80 °C). The MEA plates were incubated for 4 days at 25°C and obtained fungal culture was used to prepare spore inoculum. For each biological replicate, two MEA plates were prepared.

Spore inoculum was prepared by adding 10 mL of sterile 0.9% NaCl solution to MEA plate. Before transferring to a falcon tube, the spores were fully submerged and loosened, by careful stirring with a bacteriological loop.

Preparing nitrogen-limited broth media

The detailed composition of the nitrogen-limited broth media is described in Table 1.

Table 1 Chemical composition of the broth media.

Chemical component	Chemical formula	Concentration (g/L)		
Glucose	D(+)-glucose monohydrate	88		
Inorganic nitrogen	$(NH_4)_2SO_4$	1.5		
Magnesium	$MgSO_4 7H_2O$	1.5		
Calcium (Only for Ca1-conditions)	$CaCl_2 * 2H_2O$	0.1		
Inorganic phosphorus	Phosphate salts:	P1:	P4:	P0.5:
	KH_2PO_4	7	28	3.5
	Na_2HPO_4	2	8	1
Trace elements	$FeCl_3 6H_2O$	0.008		
	$ZnSO_4 7H_2O$	0.001		
	$CoSO_4 7H_2O$	0.0001		
	$CuSO_4 5H_2O$	0.0001		
	$MnSO_4 5H_2O$	0.0001		

For preparing the nitrogen-limited broth media, seven stock solutions of the different components were prepared (stock solution mixture can be found in Supplementary table 1 in Appendix): glucose, ammonium sulphate, magnesium + calcium, magnesium, P1, P4, P0.5, all trace elements minus $FeCl_3 6H_2O$ (TE&Fe0), and $FeCl_3 6H_2O$ (Fe). All stock solutions, except for TE&Fe0 and Fe, were autoclaved at 121 °C for 15 minutes. TE&Fe0 and Fe were sterilized using 0.45µm cellulose acetate sterile syringe filter (VWR and/or Corning Incorporated). Stock solutions were used to prepare the final broth media.

Cultivation in Duetz microtiter plate system (Duetz-MTPS)

Each biological replicate was cultivated in Duetz microtiter plate system (Duetz-MTPS) (Enzyscreen, Netherlands) consisting of 24-square polypropylene deepwell microtiter plates (MTPs), sandwich covers and clamp systems. For each treatment, three wells were utilized, and each well was inoculated with 50 µL spore inoculum and 7mL broth media. Low-evaporation sandwich covers with extra-high cover clamps were used as covers for MTPs, and MTPs were mounted in the clamp systems on the shaking platform of a Climo-Shaker ISF1-X (Kuhner Shaker). The cultivation was done at 250 rpm agitation, at 25°C for 5 days.

Harvesting biomass

After 5 days of cultivation, the produced biomass was harvested and washed, using a vacuum filtration system consisting of a Laboport N 86 KN. 18 vacuum pump (KNF), MF-Millipore gridded MCE 0.45 µm pore size 47 mm diameter filter (Merck) and a Millipore glass filter kit (Merck) (250mL glass funnel, 1000 mL side-arm flask, spring clamp, glass base and stopper). Biomass from three wells with the same treatment (i.e., same broth media) was collected and gathered in the glass funnel, on top of the filter. The biomass was washed with distilled deionized water and the washed biomass was collected into 2 mL safe-lock Eppendorf tubes, and immediately put on dry ice. Between each sample, the Millipore glass filter kit was rinsed with distilled water, and the filter was changed. The culture supernatant from each sample was collected for future examinations (outside the scope of this master thesis). Biomass samples from the MTPS were stored at -80°C.

Analysis of biomass

Chemical analysis of fungal biomass was done using gas chromatography coupled with flame ionization detector (GC-FID) for estimating total lipid content and fatty acid composition and Fourier-transform infrared spectroscopy, the high-throughput screening extension (FTIR-HTS) for estimating relative lipid and polyphosphate content. Before GC-FID and FTIR-HTS, all biomass samples showing successful RNA-extraction (Appendix, Supplementary table 2) were freeze-dried for 72 h (Labconco, USA), then stored at -20°C.

GC-FID analysis

Lipid extraction protocol

The protocol for lipid extraction was carried out according to Dzurendova et al. (2021b).
2 mL screw cap microcentrifuge tubes were filled with 250mg (+/- 30mg) acid washed glass beads (710-1180 μm diameter), 20 mg freeze-dried fungal biomass (+/- 5mg) and 500 μL chloroform. Then, 1 mg of glyceryl tritridecanoate (C13:0 triacylglycerol: TAG) internal standard solution in 100 μL hexane was added.
The tubes with the biomass were put in Precellys Evolution tissue homogenizer (Bertin Technologies, France) for homogenization with the following settings: Tube: 2 mL, Speed: 5500 rpm, Cycle: 6 x 20 s, Pause: 20. The processed biomass was transferred into glass reaction tubes by washing with 800 μL methanol-chloroform-hydrochloric acid three times (total volume: 2400 μL) and then 500 μL of methanol was added.
The reaction mixture was incubated for 90 minutes in a Stuart SBH130D/3 block heater (Cole-Parmer, UK) at 90 °C, with closed lids on the tubes. After cooling down, 1 mL of distilled water, 2 mL hexane and a small amount of anhydrous sodium sulphate was added and mixed by vortexing for 10 seconds, then the reaction tubes were centrifuged in a HERMLE High speed centrifuge Z 32 HK (HERMLE Labortechnik GmbH, Wehingen, Germany) at 4 °C for 5 minutes. The fatty acid methyl esters (FAMEs) were extracted by collecting the upper organic phase in new glass tubes. The following steps were repeated two times: Addition of 2 mL hexane-chloroform mixture, 10 s vortexing, centrifugation at 4 °C for 5 min and collection of the upper phase.
The glass tubes were placed on the block heater at 30 °C, and the solvent was evaporated under 100% nitrogen gas. After evaporation, the FAMEs were transferred into GC vials by washing the tubes with 750 μL hexane containing 0.01% butylated hydroxytoluene (BHT, Sigma-Aldrich, USA) two times (total volume: 1500 μL), each time followed by pipette mixing. The vials were stored at -20 °C until GC analysis.

GC analysis of samples

The total lipid content and fatty acid composition was determined using gas chromatography with a flame ionization detector (FID), with helium as a carrier gas. Specifics on the system: 7820A System (Agilent Technologies, USA), equipped with an Agilent J&W 121–2323DB-23 column,

20m × 180 μm × 0.20 μm. For a single sample, the total runtime was 36 minutes, 1 μL of a sample was injected, with the injector temperature of 250 °C (30:1 split ratio, with split flow 30 mL/min). The oven temperature increased to 70 °C for the first 2 min, after 8 min to 150 °C with no hold time, 230 °C in 16 min with 5 min hold time, and 245 °C in 1 min with 4 min hold time. The AgilentOpenLAB software (Agilent Technologies, USA) was used to control the measurements.

Analysis of GC data

Processing of GC data was provided by the Faculty of Science and Technology (REALTEK) at NMBU.

The external standard Supelco 37 Component FAME Mix (C4–C24 FAME mixture, Sigma-Aldrich, USA) and the internal standard C13:0 TAG were used to identify and quantify the fatty acids. The weight of individual fatty acids (FAs) was calculated based on peak areas, relative response factors (RRF) and C13:0 internal standard. Total lipid content of fungal biomass was calculated in a percentage (%) by summing up all detected fatty acids (without the weight of C13:0) for the all the samples individually in Microsoft Excel (Microsoft Excel 2019, Microsoft Corp., Redmond, WA, USA).

FTIR-HTS of fungal biomass

Homogenizing the biomass

2 mL screw cap microcentrifuge tubes were filled with 250 mg acid washed glass beads (710-1180 μm diameter), 5-6 mg of fungal biomass and 0.5 mL distilled water. The tubes were put in Precellys Evolution tissue homogenizer (Bertin Technologies, France) with the following settings: Tube: 2 mL, Speed: 5500 rpm, Cycle: 6 x 20 s, Pause: 20 s.

Preparing infrared plates

The homogenized cell suspension was transferred onto silicon 384-well FTIR plates. For each biological replicate, three technical replicates were prepared for FTIR. Each technical replicate consisted of one 10 μL drop of homogenized biomass. The FTIR plate was dried in a fume hood for approximately 1 hour.

Recording of spectra

FTIR spectra of the samples were recorded according to Dzurendova et al. (2021b), in transmission mode using a high-throughput screening extension (HTS-XT) unit coupled to a Vertex 70 FTIR spectrometer (both Bruker Optik GmbH, Leipzig, Germany). Spectra were recorded in the region between 4000 and 500 cm−1, with a spectral resolution of 6 cm−1, a digital spacing of 1.928 cm−1, and an aperture of 5 mm. For each spectrum, 64 scans were averaged. Spectra were recorded as the ratio of the sample spectrum to the spectrum of the empty IR transparent microplate. The OPUS software (Bruker Optik GmbH, Leipzig, Germany) was used for data acquisition and instrument control.

Analysis of spectra

Processing and analysis of spectra was provided by the Faculty of Science and Technology (REALTEK) at NMBU.

Data analysis was done using Orange data mining toolbox version 3.20 (University of Ljubljana, Slovenia). The preprocessing of spectra was done by using Extended multiplicative signal correction (EMSC) (with linear, quadratic, and cubic terms).

The estimation of lipid-to-protein (LP) and polyphosphate-to-protein (PP) ratios was based on bands of spectra peaks associated with protein, lipids and polyphosphates. For proteins, the amide I peak (1650 cm^{-1}) was chosen as a reference band. For lipids, the ester bond in the FTIR spectra (C=O stretching at 1745 cm^{-1}) was selected. Polyphosphates was estimated using a functional phosphate group bond (P=O stretching at 1251 cm^{-1}).

Production of RNA sequencing data

RNA extraction

RNA extraction was done using the RNeasy Plus Mini kit (Qiagen, Venlo, The Netherlands), according to the RNeasy Plus Mini Handbook's "Protocol for purification of total RNA from animal tissues". The kit contains gDNA Eliminator Spin Columns, RNeasy spin columns, Buffer RLT Plus, Buffer RW1, Buffer RPE (concentrate), RNase free water and collection tubes. Briefly, the principles of the protocol are: 1. Inactivating RNases using a highly denaturing guanidine-isothiocyanate-containing buffer in the homogenizing step. 2. Removal of genomic DNA (gDNA), without additional DNase digestion needed, through the gDNA Eliminator spin column. 3. Binding RNA to the RNeasy spin column using ethanol, before washing contaminants away. The final product is RNA molecules longer than 200 nucleotides, eluted in water. Since RNA such as 5.8S rRNA, 5S rRNA and tRNAs are shorter what 200 nucleotides, the extraction protocol results in mainly mRNAs.

Preparation of Buffers

The buffer used for homogenization was prepared by adding 10 µL β-mercaptoethanol (β-ME) per 1 mL Buffer RLT Plus. As Buffer RPE was supplied as a concentrate, a working solution was prepared by adding 4 volumes of 96-100% ethanol.

Disruption and homogenization of fungal tissue

25 (+/- 5) mg of frozen fungal tissue (kept at -80 °C) was disrupted using a mortar and pestle together with liquid nitrogen. After the material was pulverized, 650 µL of Buffer RLT Plus (containing β-ME) was added, followed by additional grinding. The lysate was pipetted into a 2 mL microcentrifuge tube and centrifuged for 3 min at maximum speed.

Removal of gDNA, followed by binding, washing, and elution of RNA

The supernatant (from the centrifuged lysate) was transferred to the gDNA Eliminator spin column placed in a 2 mL collection tube. After centrifuging for 30 sec at 10 000 rpm in a Heraeus Fresco 21 Centrifuge (Thermo Scientific, USA), the column was discarded and the flow-through was saved for the next step.

A volume equal to the flow-through of 70% ethanol (~550 µL) was added and mixed by pipetting. 600 µL of this mixture was added to the RNeasy spin column placed in a 2 mL collection tube, followed by centrifugation for 15 sec at 10 000 rpm. After this, and the following

two centrifugations, the flow-through was discarded and the collection tube was reused. 700 µL of Buffer RW1 was added to the RNeasy spin column, before centrifuging for 15 sec at 10 000 rpm to wash the spin column membrane. 500 µL of Buffer RPE was added to the RNeasy spin column, followed by centrifugation for 15 sec at 10 000 rpm to wash the spin column membrane. Then, 500 µL of Buffer RPE was added to the RNeasy spin column. To ensure removal of ethanol, it was centrifuged for 2 min at 10 000 rpm. The RNeasy spin column was placed in a new 2 mL collection tube and centrifuged at full speed for 1 min to eliminate any residual flow-through and possible carryover Buffer RPE. Following that, the RNeasy spin column was placed in a 1.5 mL Biosphere SafeSeal Tube (Sarstedt, Germany) and 30 µL of RNase-free water was added directly onto the spin column membrane, followed by centrifugation for 1 minute at 10 000 rpm to elute the RNA.

The RNeasy spin column was removed, and the SafeSeal tubes containing the eluted RNA were stored at -80 °C until shipping of samples to Novogene.

Quality control

Before storage, quality control (QC) of samples was performed using NanoDrop 8000 Spectrophotometer (Thermo Scientific, USA) and Agilent Tape Station 4150 (Agilent Technologies, USA), assessing the samples RNA concentration, purity, and integrity. QC was also carried out at Novogene, whose results differed from ours in RNA concentration. This led to only some samples being chosen for library preparation and sequencing. The summary of QC and chosen samples can be found in Supplementary table 2 in Appendix.

RNA library preparation and sequencing

To reveal the transcriptome (full range of expressed genes), the samples were sent to Novogene, a provider of genomic services using Next Generation Sequencing.

After sample quality control (QC, see Appendix), RNA library preparation and sequencing was carried out. Library preparation consisted of rRNA removal (polyA capture), followed by enrichment of single-stranded messenger RNAs (mRNAs) and reverse transcription to obtain complementary DNA (cDNA). Illumina PE150 technology (paired-end 150 basepair sequencing strategy, short read), was utilized for sequencing the cDNA.

Processing of raw RNA sequencing data

The bioinformatics pipeline nf-core/rnaseq (Ewels et al., 2020; Patel, 2022), built using the workflow manager software Nextflow (Seqera Labs, Barcelona, Spain), was used to process the raw RNAseq data. Through tools such as FastQC, Trim Galore!, STAR and Salmon, the pipeline performs quality control (QC), trimming, genome alignment and quantification, pseudo-alignment and post-processing (Figure 3).

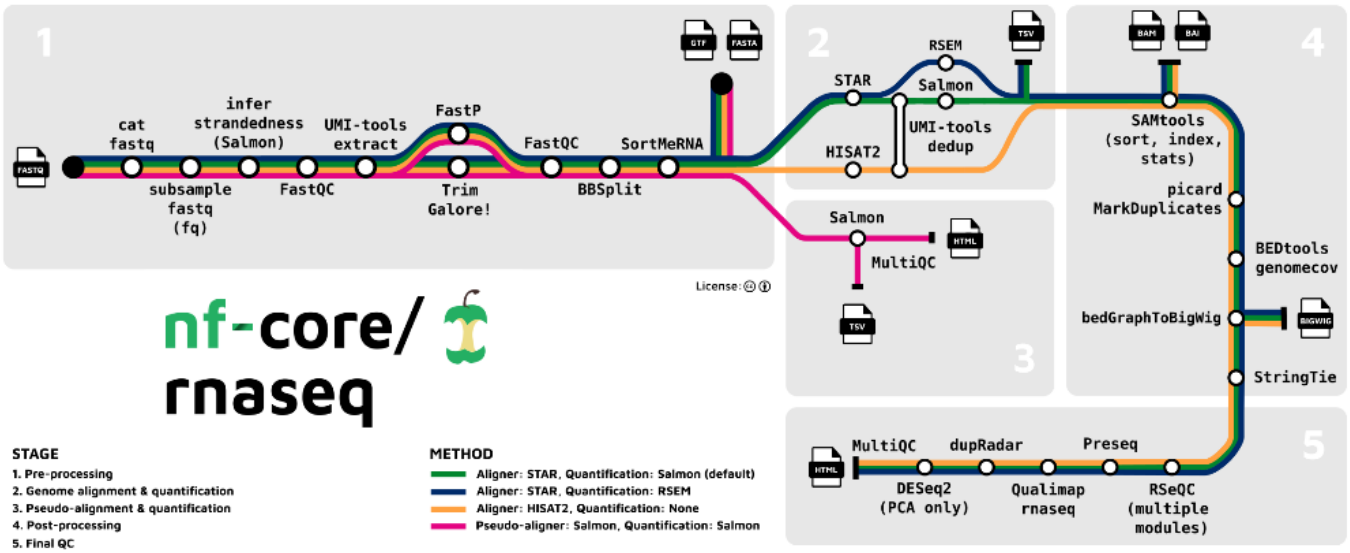

Figure 3 The workflow of nf-core/rnaseq employs several different tools and applications. Illustration: nf-core/rnaseq's homepage (Ewels et al., 2023).

The pipeline was run on NMBU's high performance computing cluster Orion using a Bash script. The inputs were: 1. A samplesheet csv-file containing paths to the raw fastq files of RNAseq data and sample names with specified library preparation strandedness (this was "reverse" for our samples). 2. A fasta file with the reference genome and a gff file with annotation for MC VI 0447. The Nextflow version 22.10.3 and the nf-core/rnaseq version 3.8 was employed for this. All parameters were set to default options, except "validate_params", which was set to 0. The output resulted in an extensive QC report and a gene expression matrix. The output file "salmon.merged.gene_counts_length_scaled.tsv" was used for downstream gene expression analyses, as recommended by nf-core/rnaseq's homepage (https://nf-co.re/rnaseq/3.11.2/output).

Genome assembly and annotation

The genome assembly and annotation for MC VI 04473 used in this thesis was produced as part of the EarthBioGenome Project, which aims to sequence all eukaryotic species. The genome was sequenced using the long-read sequencing technology from Oxford Nanopore Technologies (ONT). Genome assembly and annotation was provided by Thu-Hien To (researcher at Cigene, NMBU). Raw data were first filtered by removing short reads (<4000bp) and low quality ones (q<7), then assembled with Flye version 2.9.1 (Kolmogorov et al., 2019). The assembly have small number of contigs and L90 is 11 and probably roughly correspond to the number of chromosomes. The assemblies were evaluated with Inspector version v1.0.2 (Chen et al., 2021) and merqury version v1.3 (Rhie et al., 2020) for accessing the quality (QV) and completeness; and with Busco version 5.4.3 (Manni et al., 2021) for accessing the quantity of conserved genes. Both have high QVs, high completeness, and high Busco scores (Table 2). Annotation was done with Funannotate pipeline version v.1.8.13 (Palmer & Stajich, 2022) using the RNA-seq data generated in this thesis. This pipeline was developed specifically for annotating fungi and is widely used for genome annotation. For each one, we merged all RNA-seq samples of the corresponding strain to serve as evidence for the annotation. The assemblies were first cleaned to remove the repetitive contigs, then masked the repeat regions using the default masker tantan in funannotate. The gene models were predicted with several methods and then combined into one by Evidence Modeler. Functional annotation was run with all the implemented tools in the pipeline: Pfam, InterProScan, Eggnog, UniProtKb, Pobius, antiSMASH, MEROPS. The pipeline predicted about 12k genes, which is the expected number of genes for fungi (Mohanta & Bae, 2015).

Table 2 Detailed information on the MC VI 04473 genome assembly.

Genome Size (MB)	Nb contigs	N50 (MB)	L90	Coverage	QV inspector	QV merqury	Completeness	Busco	Busco Duplicate
41	24	4.08	11	439	47.5	53.19	95.79	98	11.3

Analysis of RNA sequencing data

Using the gene expression matrix from nf-core/rnaseq, downstream analysis of the RNAseq data was carried out in RStudio version 4.3.0 (Posit, 2023), supplemented by the online tool G:Profiler (Raudvere et al., 2019) and the command-line software tool Orthofinder version 2.5.4 (Emms & Kelly, 2019).

Differential expression analysis using DESeq2

The gene expression matrix was analyzed to reveal which genes were up- or downregulated, i.e. differentially expressed genes (DEGs), using the RStudio package DESeq2 (Love et al., 2014). This is a biostatistical tool especially designed for high-throughput sequencing assays. Based on a model using the negative binomial distribution, it calculates shrinkage estimators and variance-mean dependence in the data. Additionally, it offers normalization methods (e.g., rlog and VarianceStabilizingTransformation) to handle challenges like differences in library size, distribution of expression, sequencing depth, technical biases, and gene length.

Hypothesis testing is performed either by Wald significance test or Likelihood Ratio Test to reveal systematic differences across experimental treatments. The difference between two contrasts is presented as a Log2-transformation of the fold-change (ratio between contrasts). In short, “1” log2FoldChange (LFC) indicates that something is twice as expressed in one contrast vs. the other. The significance of the results is indicated by two different p-values: The Wald test p-value, and the p-value adjusted (padj) for multiple testing (by default after the Benjamini-Hochberg false discovery rate).

Identifying the contrast to examine in DESeq2 depends on the biological question. In this project, the contrast that seemed to be the most promising in revealing lipid-related variation in gene expression was the difference between Ca0 and Ca1 under the P0.5-condition (Ca0P0.5 vs Ca1P0.5).

Principal Component Analysis

A Principal Component Analysis (PCA) was performed on the normalized samples, using the built-in DESeq2 function plotPCA. The counts were normalized using the function Variance Stabilizing Transformation (vst) (Anders & Huber, 2010) in the RStudio package DESeq2.

The parameter ntop chooses the genes with the highest variance (across samples) for principal components (PCs), with the default setting being the ntop = 500. A larger number (ntop = 5000) was chosen, as this clarified the present patterns, making them easier to visually examine.

Biological interpretation of differentially expressed genes

Gene Onthology (GO) enrichment and yeast (*Saccharomyces cerevisiae*) orthologs were employed to examine the function of the differentially expressed genes.

A Gene ontology term is a description of the biological processes and molecular actions of a gene product. In a GO enrichment analysis, the aim is to find which GO-terms are overrepresented among a given set of genes. Based on the proportion of these genes is the gene set, and in the whole genome, a p-value is calculated, and the GO-terms are arranged according to this.

As the annotation for MC VI 04473 does not contain functional information beyond GO-terms, gene names from yeast orthologs were matched to MC VI 04473 using Orthofinder.

Lists of yeast ortholog names matched with MC VI 04473 genes were used as input in the online tool G:Profiler, and GO enrichment analysis was carried out for significantly upregulated genes, and for significantly downregulated genes.

In addition to the GO enrichment analysis, the top300 and top30 most significant genes were inspected manually, and genes related to lipid and/or calcium was singled out.

Results

Biochemical profiling of fungal biomass

Two analytical methods were used for the biochemical profiling of MC VI 04473 biomass obtained from the cultivations as described above (Ca-P conditions). GC-FID was used to obtain detailed fatty acids profile and total lipid content, while FTIR spectroscopic was used for total cellular biochemical profiling and estimating lipid to protein and polyphosphate to protein ratio of the fungal biomass.

In all treatments, the average lipid content was 30% or more of the dry cell weight (dcw) (Figure 1.1). For treatments with the reference phosphate concentration (P1) and the quadruple amount of it (P4), differences between Ca-conditions are negligible. However, for treatments with half of the phosphate reference concentration (P0.5), there is a distinct difference in lipid content between Ca1 and Ca0 and the highest average lipid content (~50% of dcw) was for Ca0P0.5.

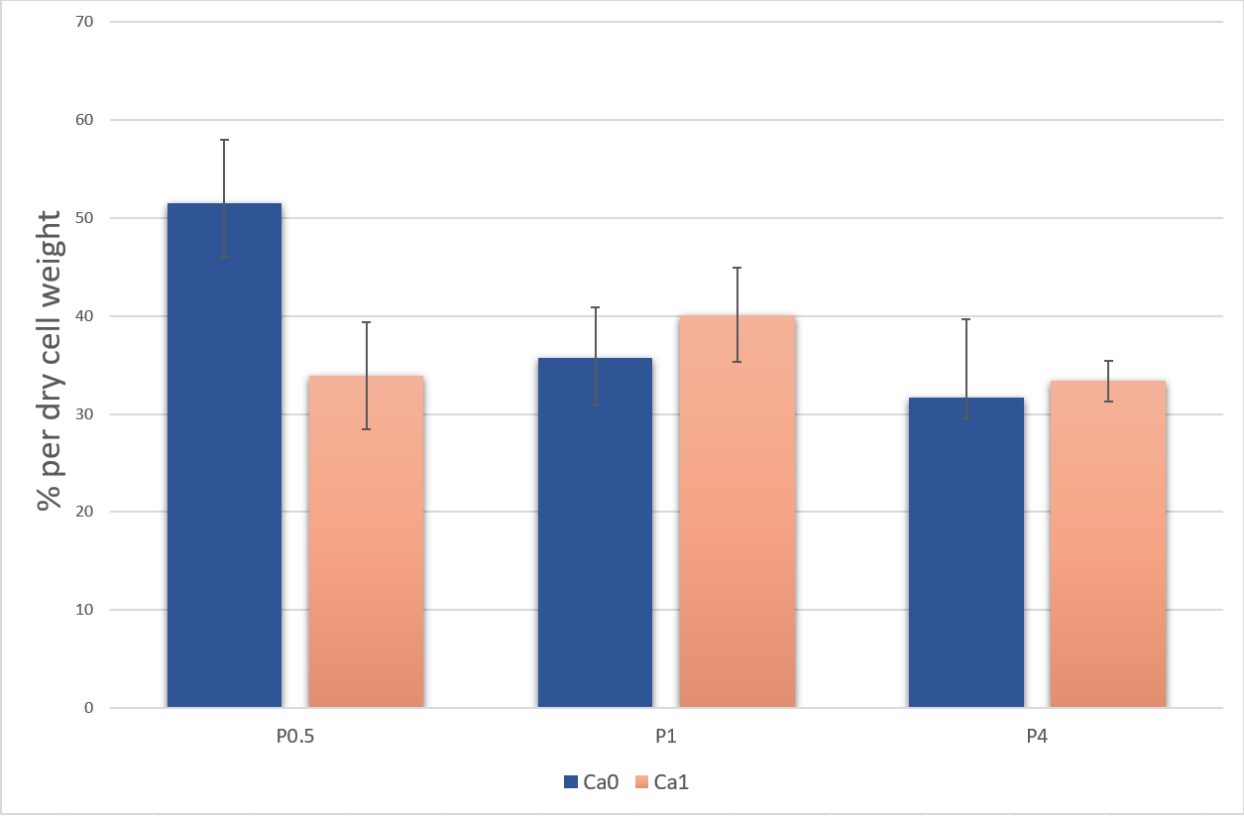

Figure 1.1 Total lipid content from each treatment, presented as percentage of dry cell weight.

The level of Ca did not have any discernible effect on the fatty acid profiles (Figure 1.2; Table 1.1). Some minor differences mainly related to the concentration of P can however be noted. In P0.5, the amount polyunsaturated fatty acids (gamma-linolenic acid and linoleic acid) were slightly greater than for other P conditions. Further, for P4 and P1 to P0.5 conditions, a gradient of slightly decreasing oleic acid can be seen, and a slight increase of palmitic acid, while palmitoleic acid were most prominent under P4 conditions.
In summary, no Ca-associated changes in fatty acid profiles were observed.

Table 1.1 Fatty acid abbreviation name (right), presenting carbon number and number of double bonds., paired with full common names for fatty acids (left). Only the most prominent fatty acids are included. Colors correspond to fatty acids in Figure 1.2.

Fatty acid abbreviation	**Full name**
C16:0	Palmitic (hexadecenoic) acid
C16:1	Palmitoleic acid
C18:0	Stearic (octadecanoic acid)
C18:1n9c	Oleic acid
C18:2n6c	Linoleic acid
C18:3n6	Gamma-linolenic acid
C24:1n9	Nervonic acid

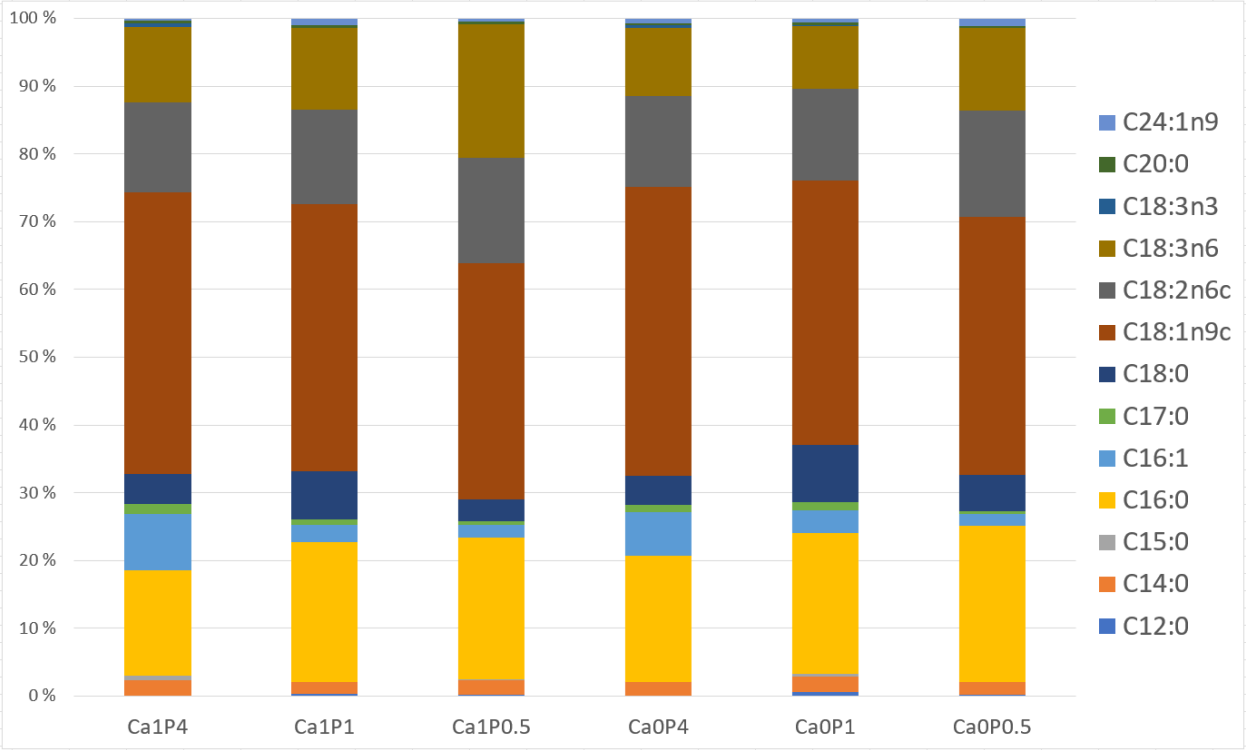

Figure 1.2 The fatty acid profile of fungal biomass obtained from each treatment.

The total biochemical composition of the fungal biomass was analyzed by Fourier transform infrared spectroscopy and relative content of lipids and polyphosphates was estimated using the peak ratio of bands associated with lipids, proteins, and phosphates, where protein peak was used as a reference due to the high stability of the total protein content in the biomass.

The ratio of lipids to proteins differed the most for Ca0-P0.5 and Ca1-P0.5 conditions and some differences were observed for P4 condition, while for P1 conditions these differences were minor (Figure 1.3). These results show Ca-dependent lipid accumulation, while P seems to play a less important role in this process.

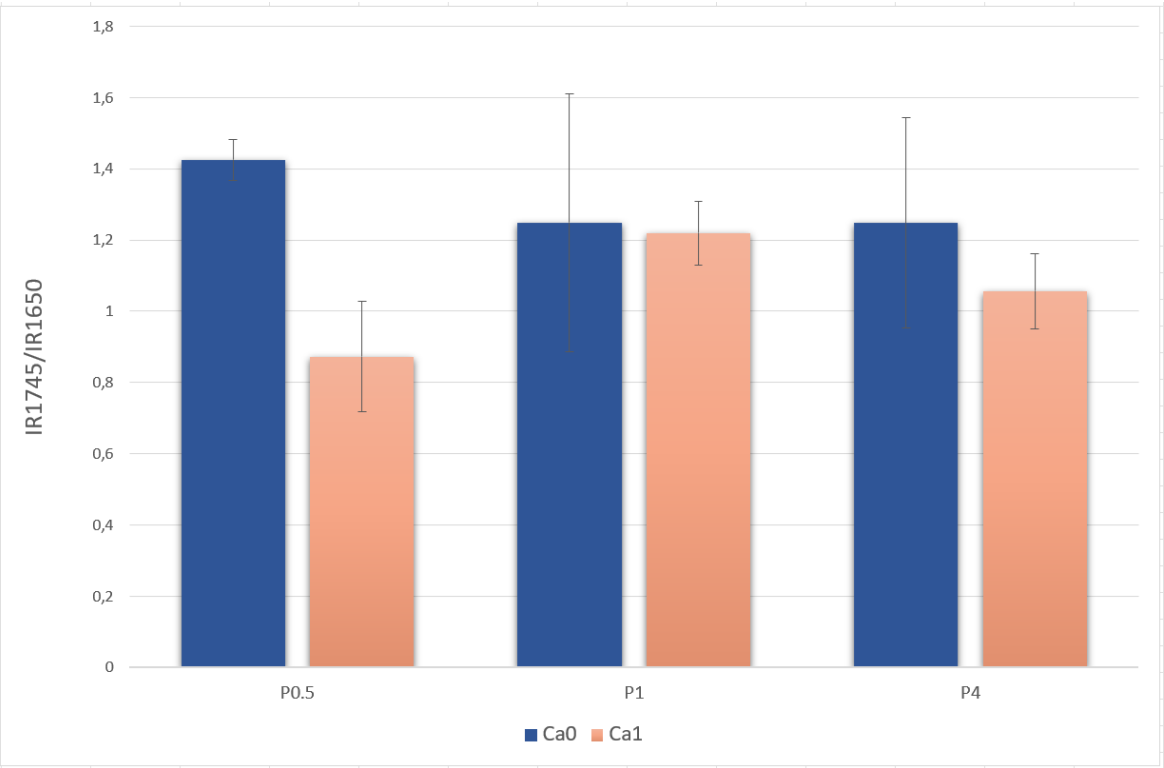

Figure 1.3 Lipid to protein ratio, calculated using the following representative peaks: ester bond C=O stretching peak at 1745 cm^{-1} for lipids, and (iii) amide I C=O stretching peak at 1650 cm^{-1} for proteins, as seen in the Y-axis.

As MC is known to accumulate polyphosphate (PolyP) (Dzurendova et al., 2021b) and presence of P in the media may affect this process, we estimated the polyphosphate to protein ratio (Figure 1.4). The fungal biomass obtained from P0.5 and P1 conditions have close to equal polyphosphate to protein ratios both between them, as well as between the Ca0 and Ca1 conditions. The highest polyphosphate ratios can be seen for biomass obtained from P4 conditions, especially for Ca1P4. The variability in accumulation of polyphosphates seems to be more P-specific, and not linked to the calcium availability.

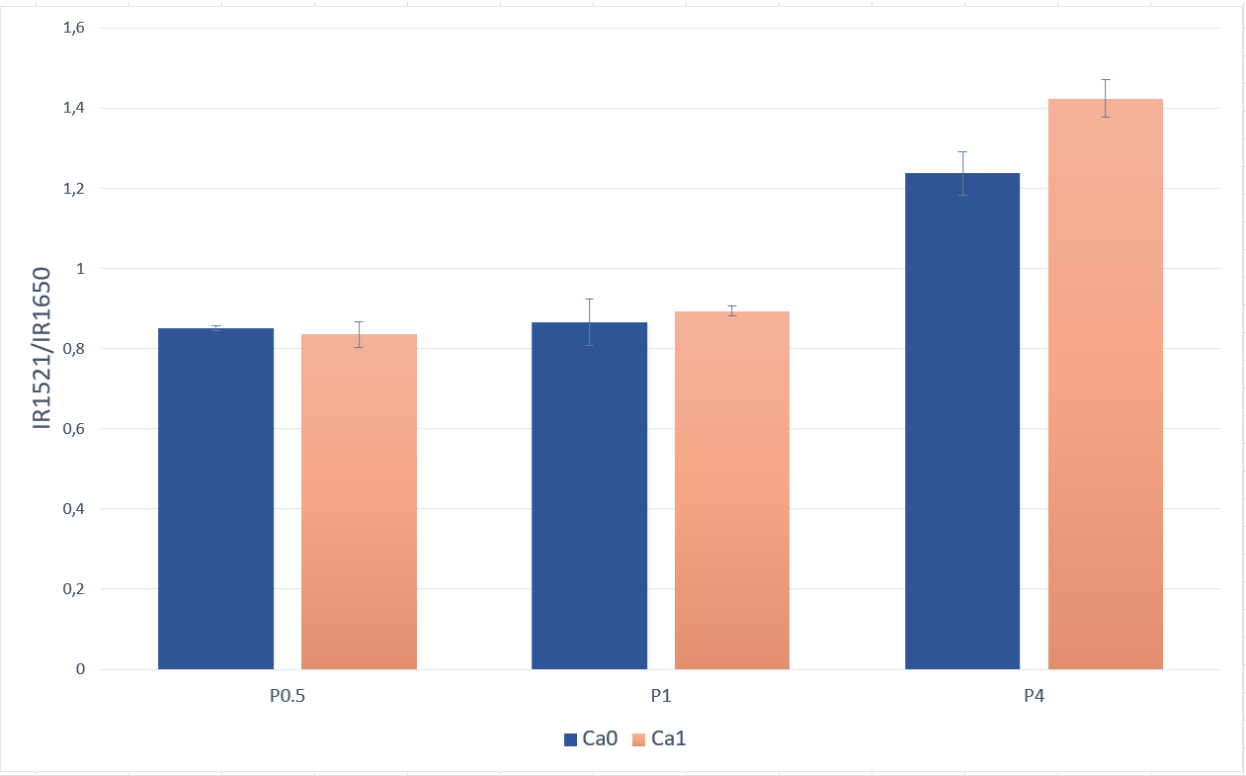

Figure 1.4 Polyphosphate to protein ratio, calculated using the following representative peaks: phosphate functional group P=O stretching peak at 1251 cm^{-1} for polyphosphates, and (iii) amide I C=O stretching peak at 1650 cm^{-1} for proteins, as seen in the Y-axis.

In summary, the chemical analysis of fungal biomass illustrates that the effect of calcium deprivation is more pronounced when combined with P depletion (P0.5). Downstream bioinformatic analyses were based on this observation.

Quality check of RNAseq data

The MultiQC report from nf-core/rnaseq showed that the obtained RNAseq data was of sufficient quality for further analyses. Most sequences had a high base call accuracy (Figure 2.1), and the sequence counts for each sample were satisfactory (Figure 2.2).

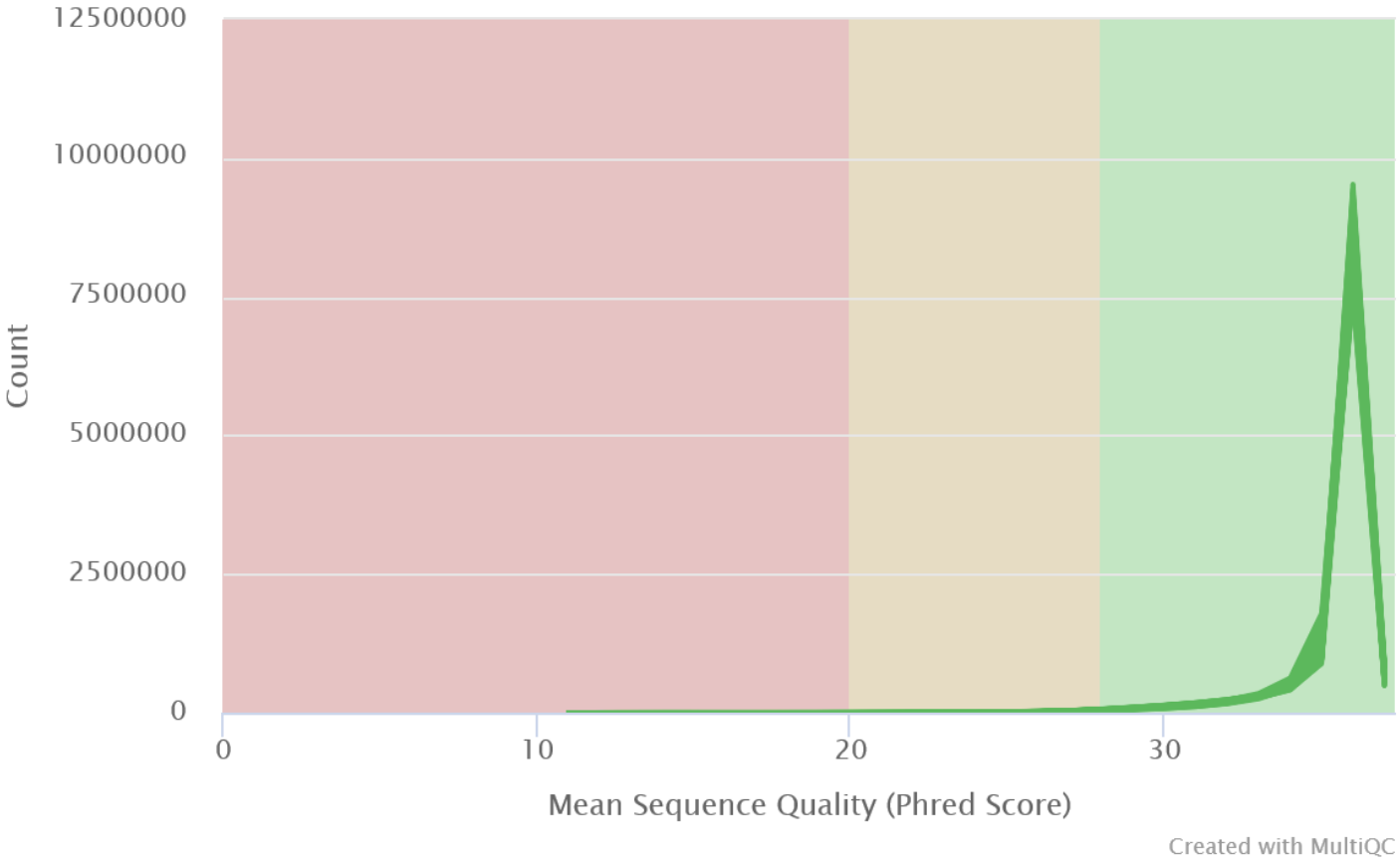

Figure 2.1 Per Sequence Quality Scores from FastQC, showing the number of sequences (y-axis) with the corresponding quality score (x-axis).

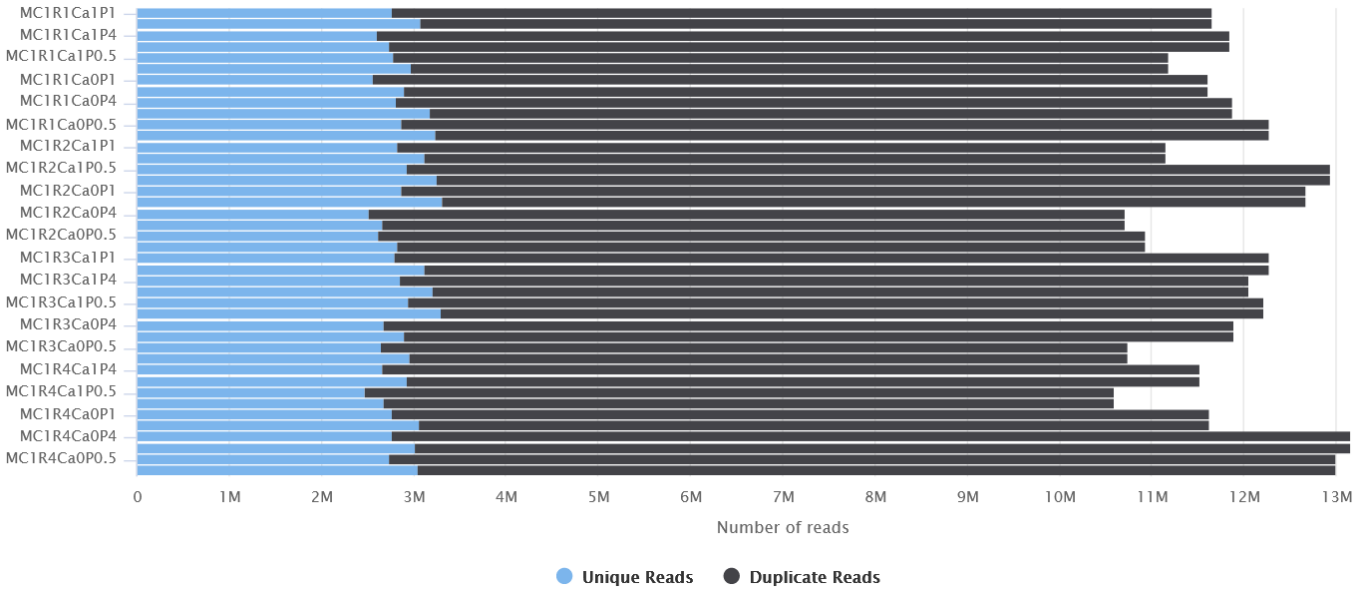

Figure 2.2 From FastQC, after adapter trimming: Number of sequencing reads per sample, and estimated duplicate reads.

Principal Component Analysis

The function plotPCA was applied to the VST-normalized counts. The PCA plots aided in visualizing how well the replicates cluster, which conditions were the main source of variation and whether there were any batch effect or outliers of concern.

The samples were clearly separated by P-condition across PC1 (Figure 2.3). It was expected that P would be the major source of variation, due to the MC's ability to store PolyP in the cell walls (Dzurendova et al., 2021b). However, the main concern was whether the data would reflect an effect of Ca-condition. There is a slight tendency for separation between Ca0 and Ca1 on PC2. To examine this further, PC3 and PC4 were also assessed.

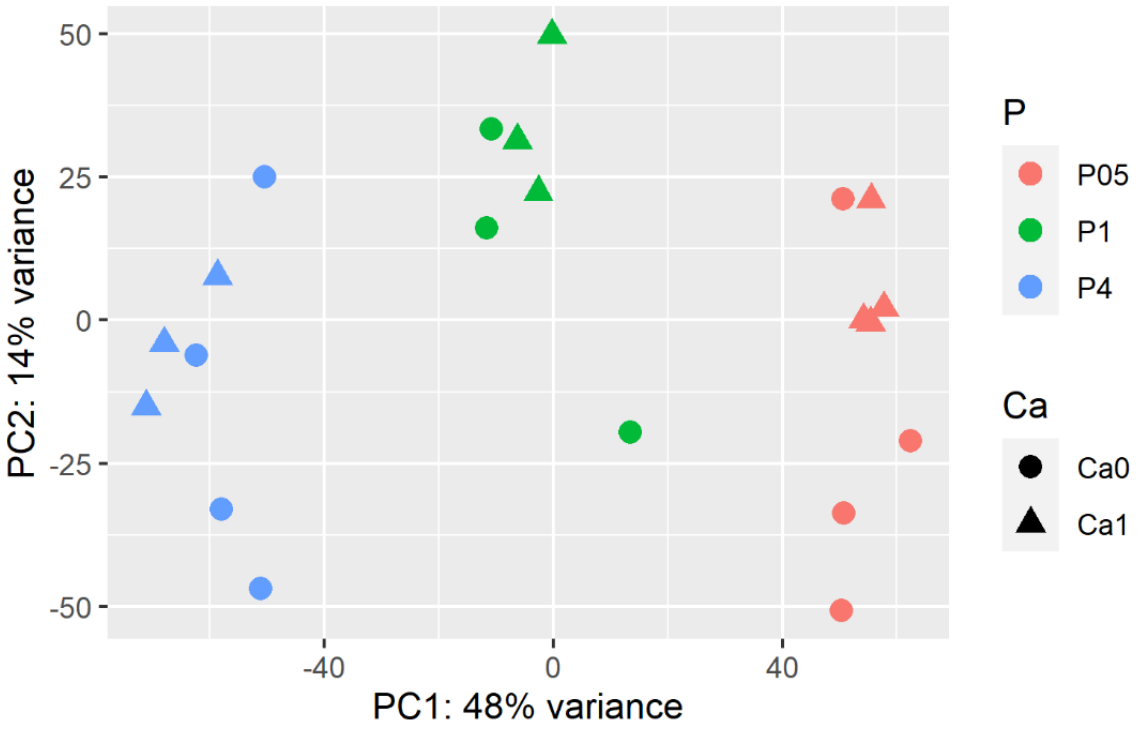

Figure 2.3 PCA plot of VST-normalized counts, with principal component 1 (PC1) against principal component 2 (PC2). PC1 explains 48% of the variance, while PC2 explains 14% of the variance.

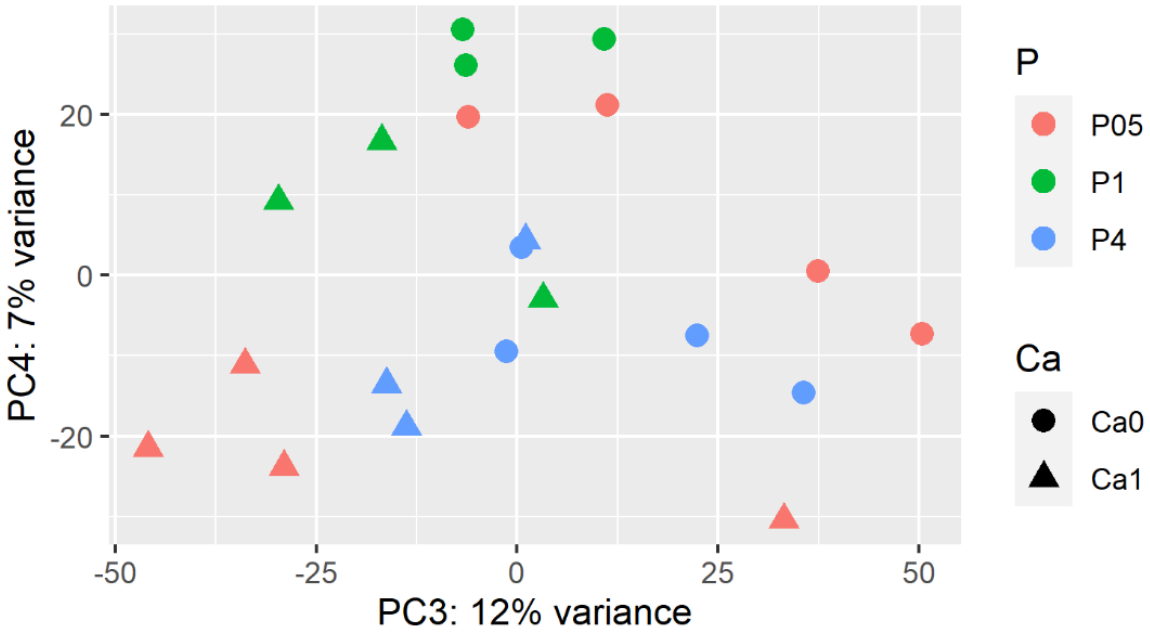

Figure 2.4 PCA plot of VST-normalized counts, with principal component 3 (PC3) against principal component 4 (PC4). PC3 explain 12% of the variance, while PC4 explains 7% of the variance.

There is a tendency of separation between Ca0 and Ca1 across PC4 (Figure 2.4) when looking at P0.5 and P1 separately. For P4, the samples are not clearly separated for Ca.
As for the unique Ca-P combinations (i.e. Ca0P0.5), the samples are somewhat clustered in both Figure 2.3 and Figure 2.4 for Ca1 conditions, while there is a bit more spread within the different Ca-conditions. In both PCA plots, two of the samples for Ca0P0.5 and Ca0P0.4 were further away from each of their treatment groups, indicating a possible batch effect. However, none of the PCA plots revealed any extreme outliers.

Differential expression analysis

The raw RNAseq counts used in the analysis contained 12343 genes. After filtering away counts smaller than 1, we were left with 11496 genes. Differential gene expression analysis was carried out on the filtered counts, for the contrast Ca0P0.5 vs Ca1P0.5. Significant DEG's were limited to those with an adjusted p-value below 0.05, and absolute Log2FoldChange above 1. The contrast resulted in 1195 upregulated genes in Ca0P0.5, and 1310 downregulated genes in Ca0P0.5 (Figure 2.5). After filtering away DEGs with and absolute log2FoldChange below 1, we were left with 491 upregulated genes, and 723 downregulated genes.

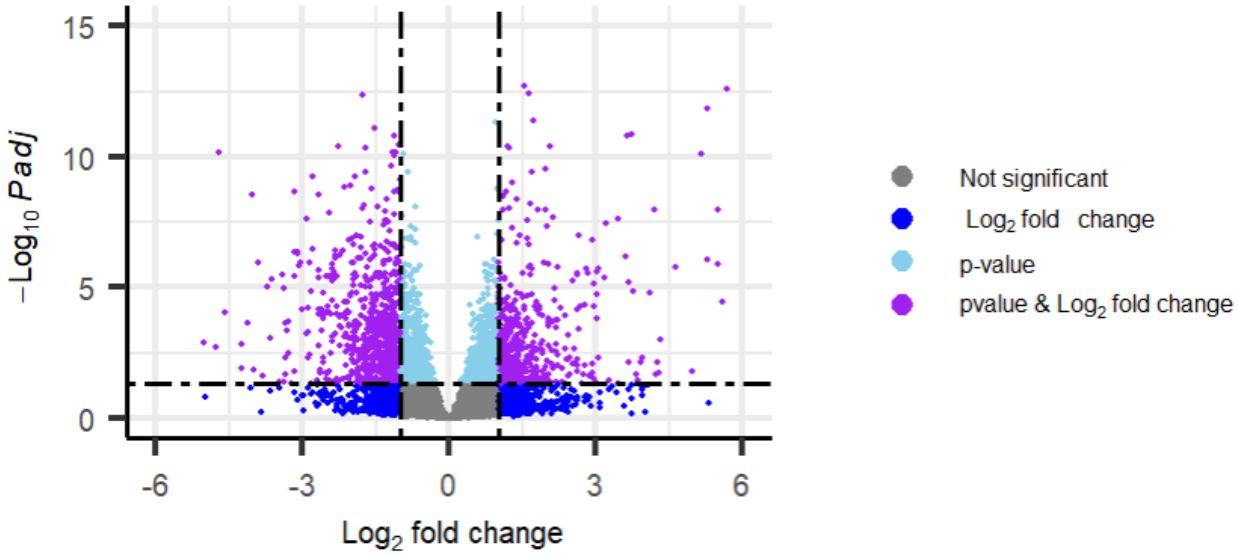

Figure 2.5 Volcano plot showing the genes and their level of significance and differential expression. Y-axis: Negative Log10 of the adjusted p-values: Higher values are more significant. X-axis: Log2FoldChange, indicating the difference in expression between Ca0 and Ca1.

There is a clear difference in expression between Ca0 and Ca1, which is illustrated in the heatmaps (Figure 2.6) both when looking at the total number of up- and downregulated genes in Ca0 as well as only the top 30 DEGs.

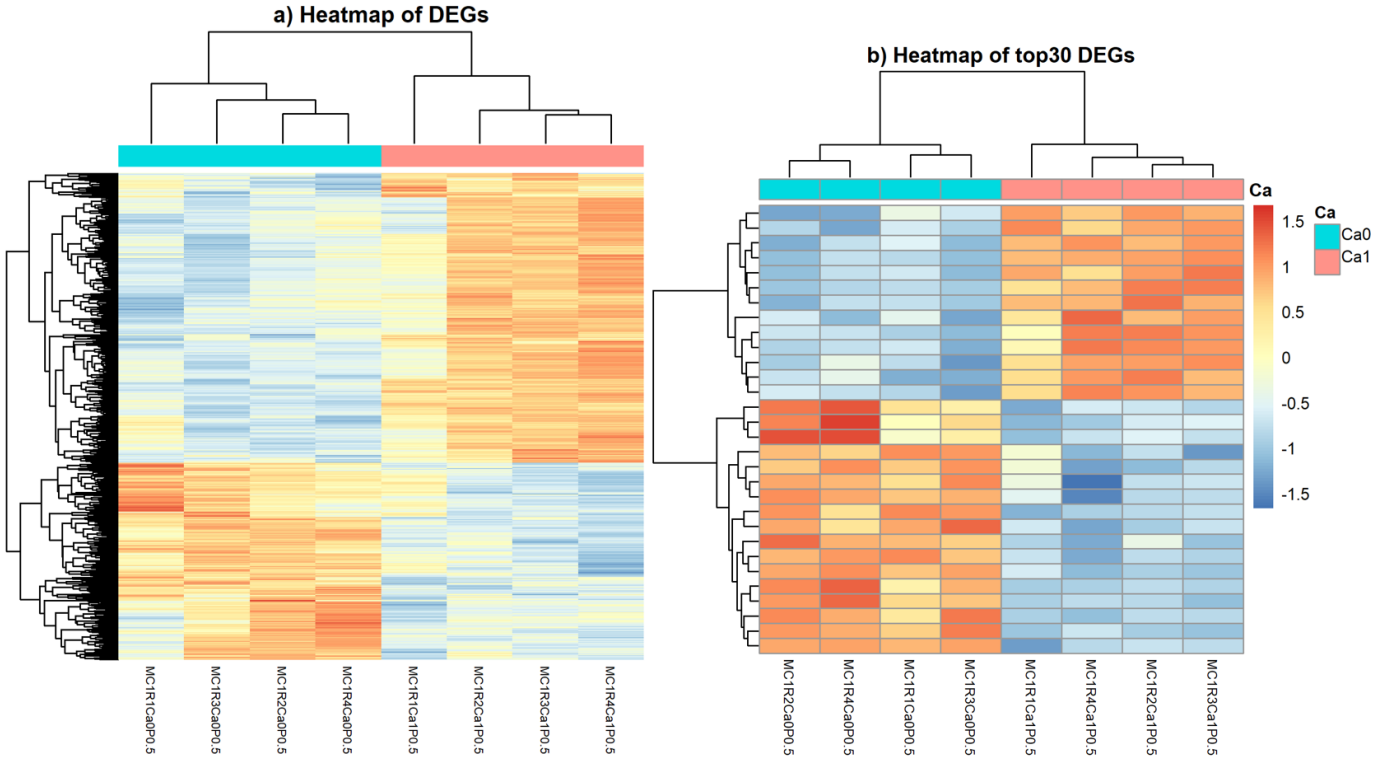

Figure 2.6 Heatmaps, showing the differential expression between Ca0 and Ca1. Blue indicates downregulation, and red indicates upregulation. Sample names explanation: MC1 = MC VI 0447, R = replicate, CaP = treatment.

GO enrichment and biological interpretation

Out of the significant DEGs (described above) 237 of the upregulated DEGs were matched with a yeast ortholog gene name. Of the downregulated DEGs, 420 were matched with a yeast ortholog gene name. The yeast ortholog gene IDs were used to perform a GO enrichment analysis, revealing the main biological functions within up and down regulated genes. The GO enrichment

analysis revealed which molecular, biological, and cellular functions were up/downregulated under the Ca0P0.5 treatment.

Among the most significant GO-terms based on the 420 downregulated DEGs were catalytic activity, small molecule metabolic process, cytoplasm, ion binding, and DNA strand elongation (Figure 2.7). Other terms worth mentioning are phospholipid biosynthetic process, organonitrogen compound catabolic process, and chaperone mediated protein folding.

ID	Source	Term ID	Term Name	p_{adj} (query_1)
1	GO:MF	GO:0003824	catalytic activity	1.708×10^{-37}
8	GO:BP	GO:0044281	small molecule metabolic process	7.807×10^{-24}
17	GO:CC	GO:0005737	cytoplasm	1.424×10^{-20}
2	GO:MF	GO:0043167	ion binding	1.164×10^{-15}
9	GO:BP	GO:0006271	DNA strand elongation involved in DNA replication	3.896×10^{-7}
10	GO:BP	GO:0008654	phospholipid biosynthetic process	4.185×10^{-5}
11	GO:BP	GO:1901565	organonitrogen compound catabolic process	1.033×10^{-4}
12	GO:BP	GO:0051086	chaperone mediated protein folding independent of cofactor	3.558×10^{-4}
18	GO:CC	GO:0042555	MCM complex	4.672×10^{-4}
19	GO:CC	GO:0030892	mitotic cohesin complex	1.590×10^{-3}
20	GO:CC	GO:0032993	protein-DNA complex	3.276×10^{-3}
21	GO:CC	GO:1990204	oxidoreductase complex	5.466×10^{-3}
22	GO:CC	GO:0005663	DNA replication factor C complex	7.627×10^{-3}
13	GO:BP	GO:0010499	proteasomal ubiquitin-independent protein catabolic process	8.791×10^{-3}
3	GO:MF	GO:0016877	ligase activity, forming carbon-sulfur bonds	1.030×10^{-2}
4	GO:MF	GO:0016624	oxidoreductase activity, acting on the aldehyde or oxo group of donors, disulfide as acceptor	1.239×10^{-2}
5	GO:MF	GO:0008061	chitin binding	1.239×10^{-2}
14	GO:BP	GO:0006950	response to stress	1.774×10^{-2}
6	GO:MF	GO:0017116	single-stranded DNA helicase activity	2.705×10^{-2}
23	GO:CC	GO:0071162	CMG complex	2.897×10^{-2}
15	GO:BP	GO:0006260	DNA replication	3.566×10^{-2}
16	GO:BP	GO:0006508	proteolysis	4.094×10^{-2}
7	GO:MF	GO:0004738	pyruvate dehydrogenase activity	4.987×10^{-2}

Figure 2.7 Summary of GO-enrichment analysis for the downregulated genes in Ca0P0.5, ordered by significance (Padj). Source GO: MF = Molecular function, BP = Biological process, CC = Cellular component.

For the 237 upregulated DEG's, the most significant GO-terms were ion binding, cell periphery, cellular processes, carbohydrate catabolic process, catalytic activity, and monocarboxylic acid metabolic process (Figure 2.8). Other molecular and biological functions worth mentioning are phosphorylation, transmembrane transporter activity, NADP+ activity, apoptotic process, P-type ion transporter activity, and peroxisomal matrix.

ID	Source	Term ID	Term Name	p_{adj} (query_1)
1	GO:MF	GO:0043167	ion binding	1.024×10^{-14}
15	GO:CC	GO:0071944	cell periphery	1.383×10^{-9}
10	GO:BP	GO:0009987	cellular process	3.232×10^{-8}
11	GO:BP	GO:0016052	carbohydrate catabolic process	2.726×10^{-7}
2	GO:MF	GO:0003824	catalytic activity	1.012×10^{-6}
12	GO:BP	GO:0032787	monocarboxylic acid metabolic process	2.128×10^{-6}
16	GO:CC	GO:0000131	incipient cellular bud site	9.133×10^{-5}
3	GO:MF	GO:0016301	kinase activity	1.367×10^{-4}
13	GO:BP	GO:0016310	phosphorylation	2.726×10^{-3}
4	GO:MF	GO:0022857	transmembrane transporter activity	3.796×10^{-3}
14	GO:BP	GO:0006915	apoptotic process	1.338×10^{-2}
5	GO:MF	GO:0008106	alcohol dehydrogenase (NADP+) activity	1.676×10^{-2}
6	GO:MF	GO:0015662	P-type ion transporter activity	1.974×10^{-2}
7	GO:MF	GO:0016898	oxidoreductase activity, acting on the CH-OH group of donors, cytochrome as acceptor	2.043×10^{-2}
8	GO:MF	GO:0004457	lactate dehydrogenase activity	2.043×10^{-2}
9	GO:MF	GO:0030695	GTPase regulator activity	2.476×10^{-2}
17	GO:CC	GO:0005782	peroxisomal matrix	2.872×10^{-2}

Figure 2.8 Summary of GO-enrichment analysis for the upregulated genes in Ca0P0.5, ordered by signifance (padj). Source GO: MF = Molecular function, BP = Biological process, CC = Cellular component.

By manually inspecting the top300 DEGs, several biologically relevant genes were identified (Table 2.1). These are directly or indirectly related to lipid synthesis and the role of calcium. Some examples are the upregulation of CMK1, FAA1, and GDP1, and the downregulation of MAE1, PEX6, BOI2 and ATP2.

The top30 DEGs included many genes of unknown function: Out of 17 upregulated genes in this list, only 5 were matched with a functional annotation, and out of the 13 downregulated genes only 9 were matched with a functional annotation. These are also included in Table 2.1.

Table 2.1 Biologically relevant DEGs from top300, and top30 DEGs are summarized in this table. First column: Gene names (yeast). Second column: A short explanation of gene function and/or gene product. Third column: Adjusted p-value, indicating the significance of the DEG. Fourth column: Log2FoldChange, where <0 indicates downregulation, and >0 indicates upregulation.

Gene name	Gene function	Adjusted p-value	Log2FoldChange
Biologically relevant DEGs from top300			
ROD1	Alpha-arrestin involved in ubiquitin-dependent endocytosis	1.26814e-07	1.61161
CMK1	Calcium/calmodulin-dependent protein kinase type I	1.0983e-06	1.92258
FAA1	Long chain fatty acyl-CoA synthetase	3.81541e-05	1.77391
ACB1	Acyl-CoA-binding protein, increases in response to DNA replication stress	3.98656e-05	1.16917
PHO13	Conserved phosphatase acting as a metabolite repair enzyme	5.66702e-06	2.53933
PGI1	phosphoglucose isomerase	4.26568e-09	1.37689
PDE2	High-affinity cyclic AMP phosphodiesterase	1.84916e-06	2.81155
MAE1	Mitochondrial malic enzyme	0.000813081	-2.15282
PHO91	Low-affinity vacuolar phosphate transporter	2.12619e-05	-1.46642
PEF1	Penta-EF-hand protein, required for polar bud growth, bind calcium and zinc	5.58819e-05	-1.53471
FAA2	Medium chain fatty acyl-CoA synthetase, localized to the peroxisome	1.66526e-05	-2.58991
PEX6	peroxisomal assembly protein	7.94145e-09	-1.4754
CSR1	Phosphatidylinositol transfer protein, has a pot ential role in regulating lipid metabolism	4.09379e-07	-2.32049
CYB5	Cytochrome, involved in the sterol and lipid biosynthesis pathways	1.5142e-05	-1.2921

ENV9	Protein proposed to be involved in vacuolar fu nctions	2.02867e-05	-2.01324
FOX2	3-hydroxyacyl-CoA dehydrogenase and enoyl-CoA hydratase, multifunctional enzyme for peroxisomal fatty acid beta-oxidation pathway	4.05801e-06	-1.72401
YBT1	Transporter of the ATP-binding cassette (ABC) family, regulates release of luminal Ca2+ stores, negative regulator of vacuolar fusion	2.68565e-08	-1.30592
BOI2	Protein implicated in polar growth	1.88885e-05	-1.39091
Upregulated genes from top30			
FKH2	Forkheadfamily transcription factor	3.18353e-23	3.38493
GPD1	NAD-dependent glycerol-3-phosphate dehydrogenase, increases when DNA replication stress	3.60857e-17	1.70164
ENT1	Epsin-like protein involved in endocytosis and actin patch assembly, activity change under DNA replication stress	3.18353e-23	1.14863
GAL10	UDP-glucose-4-epimerase	4.50973e-11	1.22887
PHO84	High-affinity inorganic phosphate (Pi) transporter	1.49782e-11	3.6442
Downregulated genes from Top30			
ATP2	Beta subunit of the F1 sector of mitochondrial F1F0 ATP synthase	3.38119e-11	-1.04486
TCP1	chaperonin-containing T-complex alpha subunit Cct1	4.92026e-11	-1.70559
MCD4	Glycosyl phosphatidyl inositol anchor synthes is	6.76513e-11	-1.16534
HTZ1	histone H2A.Z	7.71856e-12	-1.53542
CCT3	T-complex protein 1 subunit gamma	2.73196e-17	-1.13447

MCM2	MCM DNA helicase complex subunit, Protein involved in DNA replication, activated by DNA replication stress	8.80111e-11	-1.11732
STO1	Nuclear cap-binding protein subunit 1	6.56529e-11	-1.08247
THS1	threonyl-tRNA synthetase, essential cytoplasmic protein	1.81086e-17	-1.16574
EFT2	Elongation factor 2 (EF-2) U5 small nuclear ribonucleoprotein componen t	1.49782e-11	-1.11162

Discussion

Phenotypic response of MC to Ca-P conditions

The results from the biochemical profiling of MC VI 04473 showed that the combined effect of low levels of phosphorus and absence of calcium resulted in a high lipid yield (Figure 1.1 – 1.3). These findings are in accordance with what has been previously reported (Dzurendova et al., 2021b), where the same experiment was conducted for MC VI 04473 and five other Mucoromycota species. In that experiment, the pattern in lipid contents across the different P conditions, P1, P4 and P0.5, strongly resembled our results, and the contrast in lipid amount was especially pronounced between Ca0P05 and Ca1P05, as in our case (Figure 1.1; Figure 1.3).
The main components of the fatty acid profile for MC VI 04473 were the two PUFAs linoleic acid and gamma-linoleic acid, together with the saturated fatty acid palmitic acid and the mono-unsaturated oleic acid. This confirms MC VI 04473's role as a provider of fatty acids with applications in food and industry.

Genetic responses to calcium deprivation

Using differential expression analysis and GO-enrichment analysis, several DEGs and molecular functions with a potential relation to calcium starvation were identified (Figure 2.7; Figure 2.8; Table 2.1). Some of the GO-terms representing downregulated DEGs were small molecule metabolic process, cytoplasm, DNA strand elongation, phospholipid biosynthetic process, organonitrogen compound catabolic process, and chaperone mediated protein folding. This is reflected in some of the interesting findings for downregulated genes: Among these we find vacuolar functions (YBT1 and ENV9), peroxisomal FA β-oxidation pathway (FOX2, PEX2, FAA2) and proteins implicated in polar budding (BOI2), in addition to several genes for proteins involved in energy and cytoplasmic functions.
The accumulation of FAs could be explained by the downregulation of genes involved in the peroxisomal pathway, as this is associated with degradation of FAs (Dulermo et al., 2015). Polar budding and vacuolar functions could be related to changes in morphology. As MC is a dimorphic fungus, and it is a known fact that change in conditions affect the dimorphic switch, it could be assumed that morphological changes occur under calcium deprivation (Homa et al.,

2022, Lübbehüsen et al., 2003). Further, YBT1 is a negative regulator of vacuole fusion, in addition to regulating the release of luminal Ca2+ stores (Sasser et al., 2012). It seems likely that with the absence of calcium, this would be downregulated.

Other interesting genes that were downregulated were CSR1 and PEF1: CSR1 encodes phosphatidylinositol-transfer protein, which are regulators of lipid signaling (Tripathi et al., 2019). PEF1 is a calcium binding protein. Yoshibori et al. (2012) suggested that the protein Pef1p interacts and regulates coat protein complex II (COPII), which is known to play a role in the transportation of lipids and proteins from the ER to the Golgi apparatus. Both CSR1 and PEF1 are thereby highly relevant to the research questions of this thesis.

Surprisingly, the gene encoding malic enzyme (MAE1) was also downregulated. Malic enzyme is believed to be one of the main providers of NADP, which is required for lipid synthesis (Chen et al., 2015). It is unclear then why this was not upregulated under the lipid-promoting condition. One hypothesis could be that there are other NADP providers at play.

Among the GO-terms for upregulated genes we find cell periphery, cellular processes, carbohydrate catabolic process, phosphorylation, transmembrane transporter activity, NADP+ activity, and P-type ion transporter activity. During the synthesis of fatty acids, carbon is utilized, and many enzymes and precursors are required to make FAs. This is reflected in the GO-terms mentioned above, and the function of some of the interesting, upregulated genes in Ca0: The activity of cellular growth (GPD1, PGI1), polyphosphate and carbohydrate metabolism (PHO84 and PHO13), FA synthesis (FAA1), stress resistance (ACB1), and cell wall components (PGI1) (Bhalla et al., 2022; Dickinson, 1991).

The GO-terms “catalytic activity” and “Ion binding” were among the most significant terms both in the analysis of downregulated genes, and upregulated genes. This should be briefly addressed. These terms are very general, and therefore it is a possibility that they contain both genes related to lipid accumulation and/or calcium deficiency, and genes activated during presence of calcium combined with low phosphorus.

Another interesting result was the upregulation of the calmodulin encoding gene CMK1. By its regulation of the protein calcineurin, calmodulin is involved in calcium-dependent stress signaling pathways. Calmodulin can also perform essential functions in the absence of calcium, like bud growth and regulation of spindle pole body components (Cyert, 2001). Given the fact

that CMK1 was upregulated in the absence of calcium, one can therefore assume that the latter functions were activated.

Calcineurin is a serine/threonine phosphatase, with conserved mechanisms across eukaryotes. Its activation depends on the intracellular calcium concentrations (Creamer, 2020). In fungi, the role of calcineurin is related to growth, virulence, and morphogenesis (Lee et al., 2015). Based on its dependency on calcium, we considered the potential role of calcineurin in lipid accumulation. In MC, calcineurin is responsible for the transition between yeast-like growth and filamentous hyphal growth. In the case of calcineurin inactivation, MC takes on a yeast-locked phenotype (Lee et al., 2015). Recently, the morphological state of MC has been linked to its lipid accumulation trait: Yeast-like cells of MC were more rich in lipids than other cell forms (flat or swollen hyphae) (Shapaval et al., 2023).

This is an interesting observation, as it can potentially be an explanatory link between lipid accumulation and calcium availability. However, genes encoding the subunits of calcineurin were not differentially expressed in the results of this thesis. It is unclear why this was not observed, but a similar observation was made by Homa et al. (2022) in their investigation of DEGs involved in the transition between yeast-growth and hyphae under anaerobic conditions. Despite calcineurins role the morphological switch, they did not identify any differentially regulated genes corresponding to calcineurin-activity.

Attempts at understanding the relationship between lipid metabolism and calcium have been made in non-fungal species. In the model organism *Caenorhabditis elegans*, calcineurin has been linked to lipid metabolism (Y. Wang et al., 2017). Wang et al. (2017) found that in mice and *C. elegans*, the levels of calcium in the ER indirectly activates the sterol response element binding proteins (SREBPs), resulting in neutral FA synthesis. SREBPs are a transcription factors known to regulate genes involved in TAG and cholesterol metabolism. Algae has also demonstrated the ability to increase lipid content as a response to calcium starvation (Gorain et al., 2013).

In one of the few other studies of calcium effects in MC (however, not for lipid production) the effect of ions on MC using xylose as a carbon source was examined (Fonseca-Peralta et al., 2022). They concluded that certain levels of calcium and zinc could optimize the ethanol and xylitol yield. This illustrates that lipids are not the only metabolites being affected by calcium availability. As pointed out in their paper, complementary molecular analyses like metabolomics

and proteomics might elucidate which metabolic pathways and components are being limited by metal ions.

Lipid accumulation is a complex process which is regulated by many other metabolic pathways and elements. The absence of calcium might trigger a cascade of effects, like the activation of regulatory elements and transcription factors, changing both lipid synthesis and other metabolic processes. Transcriptomic analyses might therefore not always reveal genes directly involved in the response to calcium starvation, but rather general changes in e.g. the distribution and use of energy, and cell growth.

Lack of functional annotation in MC is limiting the biological interpretation of gene expression results

There are some limitations to the interpretation of the differential gene expression analysis that should be addressed. As seen in the results, only ~50% of the MC DEGs were matched with a functional gene annotation (yeast ortholog name). In the unannotated MC genes, there might lie information that would further elucidate the mechanisms of lipid accumulation as a response to calcium starvation. As for the genes matched with a yeast ortholog name, their function might not be the exact same in MC as it is in *S. cerevisiae*.

Furthermore, high-through-put omics data in GO-enrichment analysis have several sources of statistical and technical biases, and output from e.g. G:Profiler is therefore not final evidence of the gene functions of our DEGs of interest (Gaudet & Dessimoz, 2017; Timmons et al., 2015). The same can be said for genome annotations and their errors. Genome annotation technology has not been able to keep up with the rapidly evolving genome assembly technology, and the sheer numbers of draft assemblies. Automated annotation has been utilized to keep pace, but this is prone to errors (Salzberg, 2019). Another source of uncertainty lies in the RNA sequencing technology, where RNA must first be converted to cDNA before sequencing. During this process, biological information might be lost in translation (Workman et al., 2019). In the emerging technology of direct RNA sequencing, translation is not necessary, making it a promising step towards better quality genome annotations.

Conclusion

Cultivation of MC VI 04473 under calcium deprived conditions, in combination with low amount of phosphorus, was successful in triggering the lipid accumulation response. This enabled differential gene expression analysis. Under calcium deprived conditions, genes related to lipid metabolism (CSR1, FOX2, PEX2, and FAA2), polar budding and growth (BOI2, PEF1), and vacuolar functions (YBT1 and ENV9) were downregulated. The downregulation of PEF1 was one of the most interesting findings, as it is related to both calcium and lipid transportation. Genes that were upregulated under calcium deprived conditions were related to cellular growth (GPD1, PGI1, CMK1), polyphosphate/carbohydrate metabolism (PHO84 and PHO13) and stress resistance (ACB1). Despite calcineurins hypothesized role in metabolism under calcium-starvation, in addition to the yeast-hyphae transition, there were no results indicating a change in its activity.

Some of these results confirm well established knowledge on the genomic basis of lipid accumulation in MC, like the peroxisomal FA β-oxidation pathways effect on lipid yield. The discovery of downregulation in PEF1, YBT1 and CSR1 contribute some insight into the gene regulatory response to calcium starvation in MC VI 04473. However, the complete picture of how calcium and lipid metabolism are related remains somewhat unclear.

The analysis of the DEGs were based on yeast orthologs. Further studies should include more focus on functional annotation of MC VI 04473 to alleviate uncertainties in statistical and biological interpretations.

References

Anders, S., & Huber, W. (2010). Differential expression analysis for sequence count data. *Genome Biol*, *11*(10), R106-R106. https://doi.org/10.1186/gb-2010-11-10-r106

Bellou, S., Triantaphyllidou, I. E., Mizerakis, P., & Aggelis, G. (2016). High lipid accumulation in Yarrowia lipolytica cultivated under double limitation of nitrogen and magnesium. *J Biotechnol*, *234*, 116-126. https://doi.org/10.1016/j.jbiotec.2016.08.001

Bhalla, K., Qu, X., Kretschmer, M., & Kronstad, J. W. (2022). The phosphate language of fungi. *Trends Microbiol*, *30*(4), 338-349. https://doi.org/10.1016/j.tim.2021.08.002

Bonfante, P., & Venice, F. (2020). Mucoromycota: going to the roots of plant-interacting fungi. *Fungal biology reviews*, *34*(2), 100-113. https://doi.org/10.1016/j.fbr.2019.12.003

Chang, L., Tang, X., Lu, H., Zhang, H., Chen, Y. Q., Chen, H., & Chen, W. (2019). Role of Adenosine Monophosphate Deaminase during Fatty Acid Accumulation in Oleaginous Fungus Mortierella alpina. *J. Agric. Food Chem*, *67*(34), 9551-9559. https://doi.org/10.1021/acs.jafc.9b03603

Chen, H., Hao, G., Wang, L., Wang, H., Gu, Z., Liu, L., . . . Chen, Y. Q. (2015). Identification of a critical determinant that enables efficient fatty acid synthesis in oleaginous fungi. *Sci Rep*, *5*(1), 11247-11247. https://doi.org/10.1038/srep11247

Chen, Y., Zhang, Y., Wang, A. Y., Gao, M., & Chong, Z. (2021). Accurate long-read de novo assembly evaluation with Inspector. *Genome Biol*, *22*(1), 312-312. https://doi.org/10.1186/s13059-021-02527-4

Creamer, T. P. (2020). Calcineurin. *Cell Commun Signal*, *18*(1), 137-137. https://doi.org/10.1186/s12964-020-00636-4

Cyert, M. S. (2001). Genetic Analysis of Calmodulin and Its Targets in Saccharomyces cerevisiae. *Annual Review of Genetics*, *35*(1), 647-672. https://doi.org/10.1146/annurev.genet.35.102401.091302

Danielli, M., Perne, L., Jarc Jovičić, E., & Petan, T. (2023). Lipid droplets and polyunsaturated fatty acid trafficking: Balancing life and death. *Front Cell Dev Biol*, *11*, 1104725-1104725. https://doi.org/10.3389/fcell.2023.1104725

DeJarnette, C., Meyer, C. J., Jenner, A. R., Butts, A., Peters, T., Cheramie, M. N., . . . Palmer, G. E. (2021). Identification of Inhibitors of Fungal Fatty Acid Biosynthesis. *ACS Infect. Dis*, *7*(12), 3210-3223. https://doi.org/10.1021/acsinfecdis.1c00404

Dickinson, J. R. (1991). Biochemical and genetic studies on the function of, and relationship between, the PGI1- and CDC30-encoded phosphoglucose isomerases in Saccharomyces cerevisiae. *Microbiology*, *137*(4), 765-770. https://doi.org/https://doi.org/10.1099/00221287-137-4-765

Dong, T., Knoshaug, E. P., Pienkos, P. T., & Laurens, L. M. L. (2016). Lipid recovery from wet oleaginous microbial biomass for biofuel production: A critical review. *Applied energy*, *177*(C), 879-895. https://doi.org/10.1016/j.apenergy.2016.06.002

Dulermo, R., Gamboa-Meléndez, H., Ledesma-Amaro, R., Thévenieau, F., & Nicaud, J.-M. (2015). Unraveling fatty acid transport and activation mechanisms in Yarrowia lipolytica. *Biochimica et biophysica acta. Molecular and cell biology of lipids*, *1851*(9), 1202-1217. https://doi.org/10.1016/j.bbalip.2015.04.004

Dulermo, T., Tréton, B., Beopoulos, A., Kabran Gnankon, A. P., Haddouche, R., & Nicaud, J.-M. (2013). Characterization of the two intracellular lipases of Y. lipolytica encoded by TGL3 and TGL4

genes: New insights into the role of intracellular lipases and lipid body organisation. *Biochimica et biophysica acta. Molecular and cell biology of lipids*, *1831*(9), 1486-1495. https://doi.org/10.1016/j.bbalip.2013.07.001

Dzurendova, S., Losada, C. B., Dupuy-Galet, B. X., Fjær, K., & Shapaval, V. (2021a). Mucoromycota fungi as powerful cell factories for modern biorefinery. *Appl Microbiol Biotechnol*, *106*(1), 101-115. https://doi.org/10.1007/s00253-021-11720-1

Dzurendova, S., Zimmermann, B., Kohler, A., Reitzel, K., Nielsen, U. G., Dupuy-Galet, B. X., . . . Shapaval, V. (2021b). Calcium Affects Polyphosphate and Lipid Accumulation in Mucoromycota Fungi. *J Fungi (Basel)*, *7*(4). https://doi.org/10.3390/jof7040300

Emms, D. M., & Kelly, S. (2019). OrthoFinder: phylogenetic orthology inference for comparative genomics. *Genome Biol*, *20*(1), 238-238. https://doi.org/10.1186/s13059-019-1832-y

Ewels, P. A., Peltzer, A., Fillinger, S., Patel, H., Alneberg, J., Wilm, A., . . . Nahnsen, S. (2020). The nf-core framework for community-curated bioinformatics pipelines. *Nat Biotechnol*, *38*(3), 276-278. https://doi.org/10.1038/s41587-020-0439-x

Ewels, P. A., Peltzer, A., Fillinger, S., Patel, H., Alneberg, J., Wilm, A., . . . Nahnsen, S. (2023). *Introduction; nf-core/rnaseq*. Retrieved 12.05 from https://nf-co.re/rnaseq/3.8

Fazili, A. B. A., Shah, A. M., Zan, X., Naz, T., Nosheen, S., Nazir, Y., . . . Song, Y. (2022). Mucor circinelloides: a model organism for oleaginous fungi and its potential applications in bioactive lipid production. *Microb Cell Fact*, *21*(1), 29-29. https://doi.org/10.1186/s12934-022-01758-9

Fonseca-Peralta, H. M., Pineda-Hidalgo, K. V., Castro-Martínez, C., & Contreras-Andrade, I. (2022). Effect of Zinc-Calcium on Xylose Consumption by Mucor circinelloides (MN128960): Xylitol and Ethanol Yield Optimization. *Energies (Basel)*, *15*(3), 906. https://doi.org/10.3390/en15030906

Gaudet, P., & Dessimoz, C. (2017). Gene Ontology: Pitfalls, Biases, Remedies. https://doi.org/10.1007/978-1-4939-3743-1_14

Gorain, P. C., Bagchi, S. K., & Mallick, N. (2013). Effects of calcium, magnesium and sodium chloride in enhancing lipid accumulation in two green microalgae. *Environ Technol*, *34*(13-14), 1887-1894. https://doi.org/10.1080/09593330.2013.812668

Graef, M. (2018). Lipid droplet-mediated lipid and protein homeostasis in budding yeast. *FEBS Lett*, *592*(8), 1291-1303. https://doi.org/10.1002/1873-3468.12996

Homa, M., Ibragimova, S., Szebenyi, C., Nagy, G., Zsindely, N., Bodai, L., . . . Papp, T. (2022). Differential Gene Expression of Mucor lusitanicus under Aerobic and Anaerobic Conditions. *J Fungi (Basel)*, *8*(4), 404. https://doi.org/10.3390/jof8040404

Kikuchi, Y., Hijikata, N., Yokoyama, K., Ohtomo, R., Handa, Y., Kawaguchi, M., . . . Ezawa, T. (2014). Polyphosphate accumulation is driven by transcriptome alterations that lead to near-synchronous and near-equivalent uptake of inorganic cations in an arbuscular mycorrhizal fungus. *New Phytol*, *204*(3), 638-649. https://doi.org/10.1111/nph.12937

Kolmogorov, M., Yuan, J., Lin, Y., & Pevzner, P. A. (2019). Assembly of long, error-prone reads using repeat graphs. *Nat Biotechnol*, *37*(5), 540-546. https://doi.org/10.1038/s41587-019-0072-8

Lee, S. C., Li, A., Calo, S., Inoue, M., Tonthat, N. K., Bain, J. M., . . . Heitman, J. (2015). Calcineurin orchestrates dimorphic transitions, antifungal drug responses and host–pathogen interactions of the pathogenic mucoralean fungus Mucor circinelloides. *Mol Microbiol*, *97*(5), 844-865. https://doi.org/10.1111/mmi.13071

Li, Y., Steenwyk, J. L., Chang, Y., Wang, Y., James, T. Y., Stajich, J. E., . . . Rokas, A. (2021). A genome-scale phylogeny of the kingdom Fungi.

Love, M. I., Huber, W., & Anders, S. (2014). Moderated estimation of fold change and dispersion for RNA-seq data with DESeq2. *Genome Biol*, *15*(12), 550-550. https://doi.org/10.1186/s13059-014-0550-8

Lübbehüsen, T. L., Nielsen, J., & McIntyre, M. (2003). Morphology and physiology of the dimorphic fungus Mucor circinelloides (syn. M. racemosus) during anaerobic growth. *Mycol. Res*, *107*(2), 223-230. https://doi.org/10.1017/S0953756203007299

Manni, M., Berkeley, M. R., Seppey, M., Simão, F. A., & Zdobnov, E. M. (2021). BUSCO Update: Novel and Streamlined Workflows along with Broader and Deeper Phylogenetic Coverage for Scoring of Eukaryotic, Prokaryotic, and Viral Genomes. *Mol Biol Evol*, *38*(10), 4647-4654. https://doi.org/10.1093/molbev/msab199

Mohamed, H., Naz, T., Yang, J., Shah, A. M., Nazir, Y., & Song, Y. (2021). Recent Molecular Tools for the Genetic Manipulation of Highly Industrially Important Mucoromycota Fungi. *J Fungi (Basel)*, *7*(12), 1061. https://doi.org/10.3390/jof7121061

Mohanta, T. K., & Bae, H. (2015). The diversity of fungal genome. *Biol Proced Online*, *17*(1), 8-8. https://doi.org/10.1186/s12575-015-0020-z

Nagy, G., Szebenyi, C., Csernetics, Á., Vaz, A. G., Tóth, E. J., Vágvölgyi, C., & Papp, T. (2017). Development of a plasmid free CRISPR-Cas9 system for the genetic modification of Mucor circinelloides. *Sci Rep*, *7*(1), 16800-16810. https://doi.org/10.1038/s41598-017-17118-2

Naranjo-Ortiz, M. A., & Gabaldón, T. (2019). Fungal evolution: diversity, taxonomy and phylogeny of the Fungi. *Biol Rev Camb Philos Soc*, *94*(6), 2101-2137. https://doi.org/10.1111/brv.12550

NCBI. (2023). *Mucor circinelloides*. Retrieved 10.05 from https://www.ncbi.nlm.nih.gov/search/all/?term=Mucor%20circinelloides

Nosheen, S., Naz, T., Yang, J., Hussain, S. A., Fazili, A. B. A., Nazir, Y., . . . Song, Y. (2021). Role of Snf-β in lipid accumulation in the high lipid-producing fungus Mucor circinelloides WJ11. *Microb Cell Fact*, *20*(1), 52-52. https://doi.org/10.1186/s12934-021-01545-y

Ochsenreither, K., Glück, C., Stressler, T., Fischer, L., & Syldatk, C. (2016). Production Strategies and Applications of Microbial Single Cell Oils. *Front Microbiol*, *7*, 1539-1539. https://doi.org/10.3389/fmicb.2016.01539

Palmer, J. M., & Stajich, J. (2022). *Funannotate*. In (Version v1.8.13) Zenodo. https://github.com/nextgenusfs/funannotate

Patel, H. E., Phil; Peltzer, Alexander; Hammarén, Rickard; Botvinnik, Olga; Sturm, Gregor; Moreno, Denis; Vemuri, Pranathi; silviamorins; Pantano, Lorena; Binzer-Panchal, Mahesh; BABS-STP1; nf-core bot; Hanssen, Friederike; U. Garcia, Maxime; Fellows Yates, James A.; Cheshire, Chris; rfenouil; Espinosa-Carrasco, Jose; marchoeppner; Zhou, Peng; Guinchard, Sarah; Gabernet, Gisela; Zepper, Matthias; Mertes, Christian; Straub, Daniel; Hörtenhuber, Matthias; Di Tommaso, Paolo; Sven F.; Hall, George (2022). *nf-core/rnaseq: nf-core/rnaseq v3.8 - Magnesium Mongoose*. In (Version 3.8) Zenodo. https://doi.org/10.5281/zenodo.6579838

Phukhamsakda, C., Nilsson, R. H., Bhunjun, C. S., de Farias, A. R. G., Sun, Y.-R., Wijesinghe, S. N., . . . Hyde, K. D. (2022). The numbers of fungi: contributions from traditional taxonomic studies and challenges of metabarcoding. *Fungal diversity*, *114*(1), 327-386. https://doi.org/10.1007/s13225-022-00502-3

Posit, t. (2023). *RStudio: Integrated Development Environment for R. Posit Software*. In http://www.posit.co/

Raudvere, U., Kolberg, L., Kuzmin, I., Arak, T., Adler, P., Peterson, H., & Vilo, J. (2019). g:Profiler: a web server for functional enrichment analysis and conversions of gene lists (2019 update). *Nucleic Acids Res*, *47*(W1), W191-W198. https://doi.org/10.1093/nar/gkz369

Rhie, A., Walenz, B. P., Koren, S., & Phillippy, A. M. (2020). Merqury: reference-free quality, completeness, and phasing assessment for genome assemblies. *Genome Biology*, *21*(1), 1-245. https://doi.org/10.1186/s13059-020-02134-9

Roy, A., Kumar, A., Baruah, D., & Tamuli, R. (2021). Calcium signaling is involved in diverse cellular processes in fungi. *Mycology*, *12*(1), 10-24. https://doi.org/10.1080/21501203.2020.1785962

Salzberg, S. L. (2019). Next-generation genome annotation: we still struggle to get it right. *Genome Biol*, *20*(1), 92-92. https://doi.org/10.1186/s13059-019-1715-2

Sasser, Terry L., Padolina, M., & Fratti, Rutilio A. (2012). The yeast vacuolar ABC transporter Ybt1p regulates membrane fusion through Ca2+ transport modulation. *Biochemical Journal*, *448*(3), 365-372. https://doi.org/10.1042/bj20120847

Shapaval, V., Deniset-Besseau, A., Dubava, D., Dzurendova, S., Heitmann Solheim, J., & Kohler, A. (2023). Multiscale spectroscopic analysis of lipids in dimorphic and oleaginous Mucor circinelloides accommodate sustainable targeted lipid production. *Fungal Biol Biotechnol*, *10*(1), 2-2. https://doi.org/10.1186/s40694-023-00148-z

Spatafora, J. W., Chang, Y., Benny, G. L., Lazarus, K., Smith, M. E., Berbee, M. L., . . . Stajich, J. E. (2016). A phylum-level phylogenetic classification of zygomycete fungi based on genome-scale data. *Mycologia*, *108*(5), 1028-1046. https://doi.org/10.3852/16-042

Tang, X., Zhao, L., Chen, H., Chen, Y. Q., Chen, W., Song, Y., & Ratledge, C. (2015). Complete Genome Sequence of a High Lipid-Producing Strain of Mucor circinelloides WJ11 and Comparative Genome Analysis with a Low Lipid-Producing Strain CBS 277.49. *PLoS One*, *10*(9), e0137543-e0137543. https://doi.org/10.1371/journal.pone.0137543

Timmons, J. A., Szkop, K. J., & Gallagher, I. J. (2015). Multiple sources of bias confound functional enrichment analysis of global -omics data. *Genome Biol*, *16*(1), 186-186. https://doi.org/10.1186/s13059-015-0761-7

Tripathi, A., Martinez, E., Obaidullah, A. J., Lete, M. G., Lönnfors, M., Khan, D., . . . Bankaitis, V. A. (2019). Functional diversification of the chemical landscapes of yeast Sec14-like phosphatidylinositol transfer protein lipid-binding cavities. *Journal of Biological Chemistry*, *294*(50), 19081-19098. https://doi.org/https://doi.org/10.1074/jbc.RA119.011153.

Walker, G. M., & White, N. A. 2017. Introduction to Fungal Physiology, in: Kavanagh, K. (Ed.), *Fungi*. John Wiley & sons, Inc., Hoboken, NJ, USA, pp. 1-35. https://doi.org/https://doi.org/10.1002/9781119374312.ch1

Wang, S., Chen, H., Tang, X., Zhang, H., Chen, W., & Chen, Y. Q. (2017). Molecular tools for gene manipulation in filamentous fungi. *Appl Microbiol Biotechnol*, *101*(22), 8063-8075. https://doi.org/10.1007/s00253-017-8486-z

Wang, W.-A., Liu, W.-X., Durnaoglu, S., Lee, S.-K., Lian, J., Lehner, R., . . . Michalak, M. (2017). Loss of Calreticulin Uncovers a Critical Role for Calcium in Regulating Cellular Lipid Homeostasis. *Sci Rep*, *7*(1), 5941-5915. https://doi.org/10.1038/s41598-017-05734-x

Wang, Y., Xie, C., Diao, Z., & Liang, B. (2017). Calcineurin Antagonizes AMPK to Regulate Lipolysis in Caenorhabditis elegans. *Molecules*, *22*(7), 1062.

Wolff, A. M., Appel, K. F., Petersen, J. B., Poulsen, U., & Arnau, J. (2002). Identification and analysis of genes involved in the control of dimorphism in Mucor circinelloides (syn. racemosus). *FEMS Yeast Res*, *2*(2), 203-213. https://doi.org/10.1111/j.1567-1364.2002.tb00085.x

Workman, R. E., Tang, A. D., Tang, P. S., Jain, M., Tyson, J. R., Razaghi, R., . . . Timp, W. (2019). Nanopore native RNA sequencing of a human poly(A) transcriptome.

Xia, C., Zhang, J., Zhang, W., & Hu, B. (2011). new cultivation method for microbial oil production: cell pelletization and lipid accumulation by Mucor circinelloides. *Biotechnol Biofuels*, *4*(1), 15-15. https://doi.org/10.1186/1754-6834-4-15

Yang, J., Cánovas-Márquez, J. T., Li, P., Li, S., Niu, J., Wang, X., . . . Song, Y. (2021). Deletion of Plasma Membrane Malate Transporters Increased Lipid Accumulation in the Oleaginous Fungus Mucor circinelloides WJ11. *J. Agric. Food Chem*, *69*(33), 9632-9641. https://doi.org/10.1021/acs.jafc.1c03307

Yoshibori, M., Yorimitsu, T., & Sato, K. (2012). Involvement of the Penta-EF-Hand Protein Pef1p in the Ca.sup.2+-Dependent Regulation of COPII Subunit Assembly in Saccharomyces cerevisiae. *PloS one*, *7*(7), e40765. https://doi.org/10.1371/journal.pone.0040765

Zan, X., Tang, X., Chu, L., & Song, Y. (2018). Dual Functions of Lip6 and Its Regulation of Lipid Metabolism in the Oleaginous Fungus Mucor circinelloides. *J. Agric. Food Chem*, *66*(11), 2796-2804. https://doi.org/10.1021/acs.jafc.7b06024

Zhang, X.-Y., Li, B., Huang, B.-C., Wang, F.-B., Zhang, Y.-Q., Zhao, S.-G., . . . Wang, Z.-P. (2022). Production, Biosynthesis, and Commercial Applications of Fatty Acids From Oleaginous Fungi. *Front Nutr*, *9*, 873657-873657. https://doi.org/10.3389/fnut.2022.873657

Appendix

Supplementary table 1 Each of the stock solutions described below were combined to create the six different growth medias for MC VI 04473.

Stock solutions	Mass (g) / volume of water (mL)	Volumes from stocks for a 100 mL broth media (mL)
D(+)-glucose monohydrate	88 / 600	60
$(NH_4)_2SO_4$	1.5 / 100	10
Mg + Ca	1.5 + 0.1 / 100	10 (from one of them, depending on which Ca-condition)
Mg	1.5 / 100	
P1	7 + 2 / 200	20 (from one of them, depending on which P-condition)
P4	28 + 8 / 200	
P0.5	3.5 + 1 / 200	
Fe	0.08 / 10	0.1
TE&Fe0	tot. g / 10	
(Zn+	0.01	0.1
Co SO_4+	0.001	
Cu SO_4+	0.001	
Mn SO_4)	0.001	

Supplementary table 2 Summary of Novogene's QC of samples. Sample name: R = replicate, Ca = calcium condition, P = phosphorus condition. RIN = RNA integrity number (range 1-10). Sample QC result: Pass = samples of good quality for sequencing. Hold = samples of mediocre quality for sequencing. Fail = samples with too low concentration, these were not sequenced.

Sample name	RNA concentration (ng/ μL)	RIN	Sample QC result
R1Ca1P1	151.54	9.7	Pass
R1Ca1P4	33.04	10	Pass
R1Ca1P0.5	27.74	10	Pass
R1Ca0P1	40.17	9.2	Pass
R1Ca0P4	47.10	10	Pass
R1Ca0P05	54.45	10	Pass
R2Ca1P1	14.70	8.4	Hold
R2Ca1P4	2.08	8.9	Fail
R2Ca1P0.5	9.37	9.1	Hold
R2Ca0P1	10.38	7.5	Hold
R2Ca0P4	16.02	10	Hold
R2Ca0P05	16.27	9.1	Hold
R3Ca1P1	86.12	10	Pass
R3Ca1P4	38.28	9.3	Pass
R3Ca1P0.5	12.47	9.3	Hold
R3Ca0P1	1.89	10	Fail
R3Ca0P4	8.19	10	Hold
R3Ca0P05	32.37	10	Pass
R4Ca1P1	2.51	10	Fail
R4Ca1P4	7.67	10	Hold
R4Ca1P0.5	12.64	9.5	Hold
R4Ca0P1	9.79	9.8	Hold
R4Ca0P4	14.68	10	Hold
R4Ca0P05	25.35	9.8	Pass

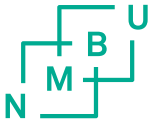

Norges miljø- og biovitenskapelige universitet
Noregs miljø- og biovitskapelege universitet
Norwegian University of Life Sciences

Postboks 5003
NO-1432 Ås
Norway